Electronic Supplementary Material (ESI) for New Journal of Chemistry.
This journal is © The Royal Society of Chemistry and the Centre National de la Recherche Scientifique 2023

Electronic Supplementary Information

Regioselective 2,3-Disubstituted Porphyrins: Synthesis, Spectral, Structural and Electrochemical Properties

Waseem Arif and Ravi Kumar*

Department of Chemistry, National Institute of Technology Srinagar, 190006, Jammu and Kashmir, India.

Table of Contents (TOC)

Figure S1. B3LYP/6-31G optimized geometries showing top as well as side views of $H_2TPP(PE)_2$ (**1a** and **1b**) and $H_2TPP(Ph)_2$ (**1d** and **1e**), respectively. In side view, the β-substituents and *meso*-phenyl groups are not shown for clarity. The displacement of porphyrin-core atoms in Å from the mean plane are shown in figures **1c** and **1f** for $H_2TPP(PE)_2$ and $H_2TPP(Ph)_2$, respectively. Color codes for atoms: C (black), N (blue) and H (white).

Figure S2. B3LYP/6-31G optimized geometries showing top as well as side views of $H_2TPP(CH_3)_2$ (**1a** and **1b**) and $H_2TPP(Br)_2$ (**1d** and **1e**), respectively. In side view, the β-substituents and *meso*-phenyl groups are not shown for clarity. The displacement of porphyrin-core atoms in Å from the mean plane are shown in figures **1c** and **1f** for $H_2TPP(CH_3)_2$ and $H_2TPP(Br)_2$, respectively. Color codes for atoms: C (black), N (blue), H (white). and Br (parrot-green).

Figure S3. B3LYP/6-31G optimized geometries showing Frontier Molecular Orbitals (FMOs) of $H_2TPP(PE)_2$ (1a) and $H_2TPP(Ph)_2$ (1b), respectively.

Figure S4. B3LYP/6-31G optimized geometries showing Frontier Molecular Orbitals (FMOs) of $H_2TPP(CH_3)_2$ (1a) and $H_2TPP(Br)_2$ (1b), respectively.

Figure S5. B3LYP/6-31G optimized geometries showing direction of dipole moment of $H_2TPP(PE)_2$ (1a), $H_2TPP(Ph)_2$ (1b), $H_2TPP(CH_3)_2$ (1c) and $H_2TPP(Br)_2$ (1d), respectively.

Figure S6. Molecular orbital energy level diagrams of $H_2TPP(Br)_2$ obtained at the B3LYP/6-31G basis set (Gaussian 16 package).

Figure S7. UV- Visible spectra of $CuTPP(X)_2$ (X = CH_3, Ph, PE) derivatives in CH_2Cl_2.

Figure S8. UV- Visible spectra of $NiTPP(X)_2$ (X = CH_3, Ph, PE) derivatives in CH_2Cl_2.

Figure S9. UV- Visible spectra of $ZnTPP(X)_2$ (X = CH_3, Ph, PE) derivatives in CH_2Cl_2.

Figure S10. UV- Visible spectra of $CoTPP(X)_2$ (X = CH_3, Ph, PE) derivatives in CH_2Cl_2.

Figure S11. Fluorescence spectra of $ZnTPP(X)_2$ (X = CH_3, Ph, PE) derivatives in CH_2Cl_2 at 298 K.

Figure S12. Cyclic voltammograms of $MTPP(PE)_2$ [M= Cu(II), Zn(II), Ni(II) and Co(II)] (~1 mM) in CH_2Cl_2 containing 0.1 M TBAPF6 using Ag/AgCl as reference electrode with a scan rate of 0.10 V/s at 298 K.

Figure S13. Cyclic voltammograms of (a) $CuTPP(X)_2$ [X= CH_3, Ph, Br and PE] (b) $NiTPP(X)_2$ [X= CH_3, Ph, Br and PE] (~1 mM) in CH_2Cl_2 containing 0.1 M $TBAPF_6$ using Ag/AgCl as reference electrode with a scan rate of 0.10 V/s at 298 K.

Figure S14. Cyclic voltammograms of (a) $CoTPP(X)_2$ [X= CH_3, Ph, Br and PE] (b) $ZnTPP(X)_2$ [X= CH_3, Ph, Br and PE] (~1 mM) in CH_2Cl_2 containing 0.1 M $TBAPF_6$ using Ag/AgCl as reference electrode with a scan rate of 0.10 V/s at 298 K.

Figure S15. ^1H NMR spectrum of $H_2TPP(Br)_2$ in $CDCl_3$ at 298 K.

Figure S16. ^1H NMR spectrum of $ZnTPP(Br)_2$ in $CDCl_3$ at 298 K.

Figure S17. ^1H NMR spectrum of $NiTPP(Br)_2$ in $CDCl_3$ at 298 K.

Figure S18. ^1H NMR spectrum of $H_2TPP(CH_3)_2$ in $CDCl_3$ at 298 K.

Figure S19. ^1H NMR spectrum of $NiTPP(CH_3)_2$ in $CDCl_3$ at 298 K.

Figure S20. ^1H NMR spectrum of $ZnTPP(CH_3)_2$ in $CDCl_3$ at 298 K.

Figure S21. ^1H NMR spectrum of $H_2TPP(Ph)_2$ in $CDCl_3$ at 298 K.

Figure S22. ^1H NMR spectrum of $ZnTPP(Ph)_2$ in $CDCl_3$ at 298 K.

Figure S23. ^1H NMR spectrum of $NiTPP(Ph)_2$ in $CDCl_3$ at 298 K.

Figure S24. ^1H NMR spectrum of $H_2TPP(PE)_2$ in $CDCl_3$ at 298 K.

Figure S25. ^1H NMR spectrum of $ZnTPP(PE)_2$ in $CDCl_3$ at 298 K.

Figure S26. ^1H NMR spectrum of $NiTPP(PE)_2$ in $CDCl_3$ at 298 K.

Figure S27. HRMS spectrum of $H_2TPP(Br)_2$.

Figure S28. HRMS spectrum of $ZnTPP(Br)_2$.

Figure S29. HRMS spectrum of $H_2TPP(CH_3)_2$.

Figure S30. HRMS spectrum of $CoTPP(CH_3)_2$.

Figure S31. HRMS spectrum of $ZnTPP(CH_3)_2$.

Figure S32. HRMS spectrum of $NiTPP(CH_3)_2$.

Figure S33. HRMS spectrum of $H_2TPP(PE)_2$.

Figure S34. HRMS spectrum of $CoTPP(PE)_2$.

Figure S35. HRMS spectrum of $H_2TPP(Ph)_2$.

Figure S36. HRMS spectrum of $CuTPP(Ph)_2$.

Figure S37. HRMS spectrum of $CoTPP(Ph)_2$.

Figure S38. HRMS spectrum of $ZnTPP(Ph)_2$.

Table S1. Crystal structure data of $H_2TPP(CH_3)_2$ and $CuTPP(PE)_2$.

Table S2. Selected bond lengths (Å) and bond angles (º) of $H_2TPP(CH_3)_2$ and $CuTPP(PE)_2$.

Table S3. Selected bond lengths (Å), bond angles (º) and calculated dipole moment for the B3LYP/6-31G optimised geometries of $H_2TPP(X)_2$ (X = PE, Br, Ph and CH_3).

Table S4. Optical absorption spectral data of all the newely synthesized regioselective *β*-disubstituted free base porphyrins as well as their metal complexes.

Table S5. Fluorescence spectral data and quantum yield of $MTPP(X)_2$ (M = H_2, Zn, and X = CH_3, Ph, PE) derivatives in CH_2CL_2 at 1298 K.

Table S6. Electrochemical redox data of Regioselective *β*-disubstituted porphyrins and their metal complexes $MTPP(X)_2$ [M = H_2, Cu(II), Ni(II) & Zn(II), X = CH_3, Ph, PE & Br]. in CH_2Cl_2 containing 0.1 M $TBAPF_6$ with a scan rate of 0.1 V/s at 298 K.

Table S1. Crystal structure data of $H_2TPP(CH_3)_2$ and $CuTPP(PE)_2$.

	$CuTPP(PE)_2$	**$H_2TPP(CH_3)_2$.**
Empirical formula	$C_{60}H_{36}CuN_4$	$C_{46}H_{34}N_4$
Formula wt.	876.47	642.77
Crystal system	Triclinic	Monoclinic
Space group	P-1	$P2_1/n$
a (Å)	11.6718(5)	13.9752(18)
b (Å)	13.6174(7)	18.392(3)
c (Å)	15.3876(7)	14.596(2)
α (º)	66.9110(10)	90
β (º)	82.2880(10)	116.631(4)
γ (º)	67.6690(10)	90
Volume ($Å^3$)	2080.75(17)	3353.5(8)
Z	2	4
D_{calc} (g/cm^3)	1.399	1.273
Wavelength (Å)	0.71073	0.71073
T (˚C)	296.15 K	273.15 K
No. of total reflns.	26360	53314
No. of indepnt.reflns.	7316	8319
R^a	0.0291	0.0563
R^b	0.0287	0.0385
CCDC	2237993	2242270

Table S2. Selected bond lengths (Å) and bond angles (º) of $CuTPP(PE)_2$ and $H_2TPP(CH_3)_2$.

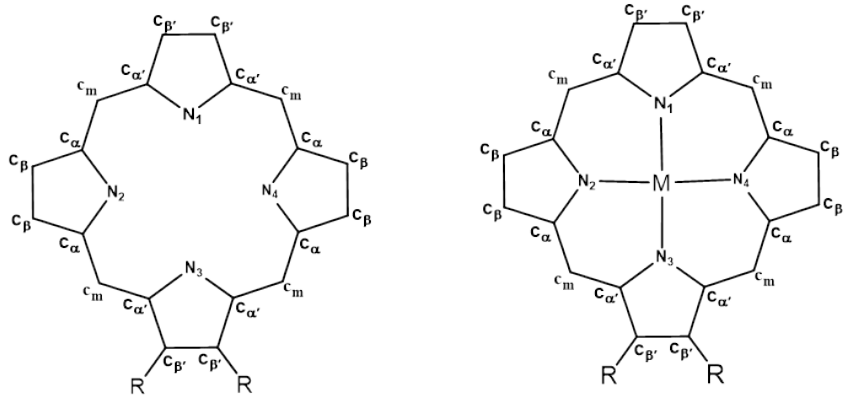

Bond Length (Å)

	$CuTPP(PE)_2$	**$H_2TPP(CH_3)_2$**
M-N	1.979	-
M-N′	2.017	-
N-C_α	1.381	1.374
N′-C_α	1.386	1.375
C_α-C_β	1.442	1.454
$C_{\alpha'}$-$C_{\beta'}$	1.446	1.441
C_β-C_β	1.344	1.347
$C_{\beta'}$-$C_{\beta'}$	1.367	1.370
C_α-C_m	1.397	1.406
$C_{\alpha'}$-C_m	1.396	1.403
ΔC_β (Å)[a]	0.287	0.162
Δ24 (Å)[b]	0.173	0.096
ΔMetal (Å)	0.013	-

Bond Angle (deg)

M-N-C_α	127.23	-
M-N′-C_α	126.77	-
N-M-N	177.04	-
N′-M-N′	177.23	-
N-C_α-C_m	125.94	126.64
N′-$C_{\alpha'}$-C_m	125.48	124.89
N-C_α-C_β	109.94	110.27
N′-$C_{\alpha'}$-$C_{\beta'}$	110.02	107.48
C_β- C_α-C_m	124.02	122.93
$C_{\beta'}$- $C_{\alpha'}$-C_m	124.47	125.85
C_α-C_m-$C_{\alpha'}$	123.35	125.69
C_α-C_β-C_β	107.26	106.83
$C_{\alpha'}$-$C_{\beta'}$-$C_{\beta'}$	106.86	107.72
C_α-N-C_α	105.46	105.75
$C_{\alpha'}$-N- $C_{\alpha'}$	106.21	109.57

[a]ΔC_β refers to the mean plane displacement of the β-pyrrole carbons

[b]Δ24 refers to the mean plane deviation of 24-atom core

esd's for all given bond length and bond angles are ± 6%

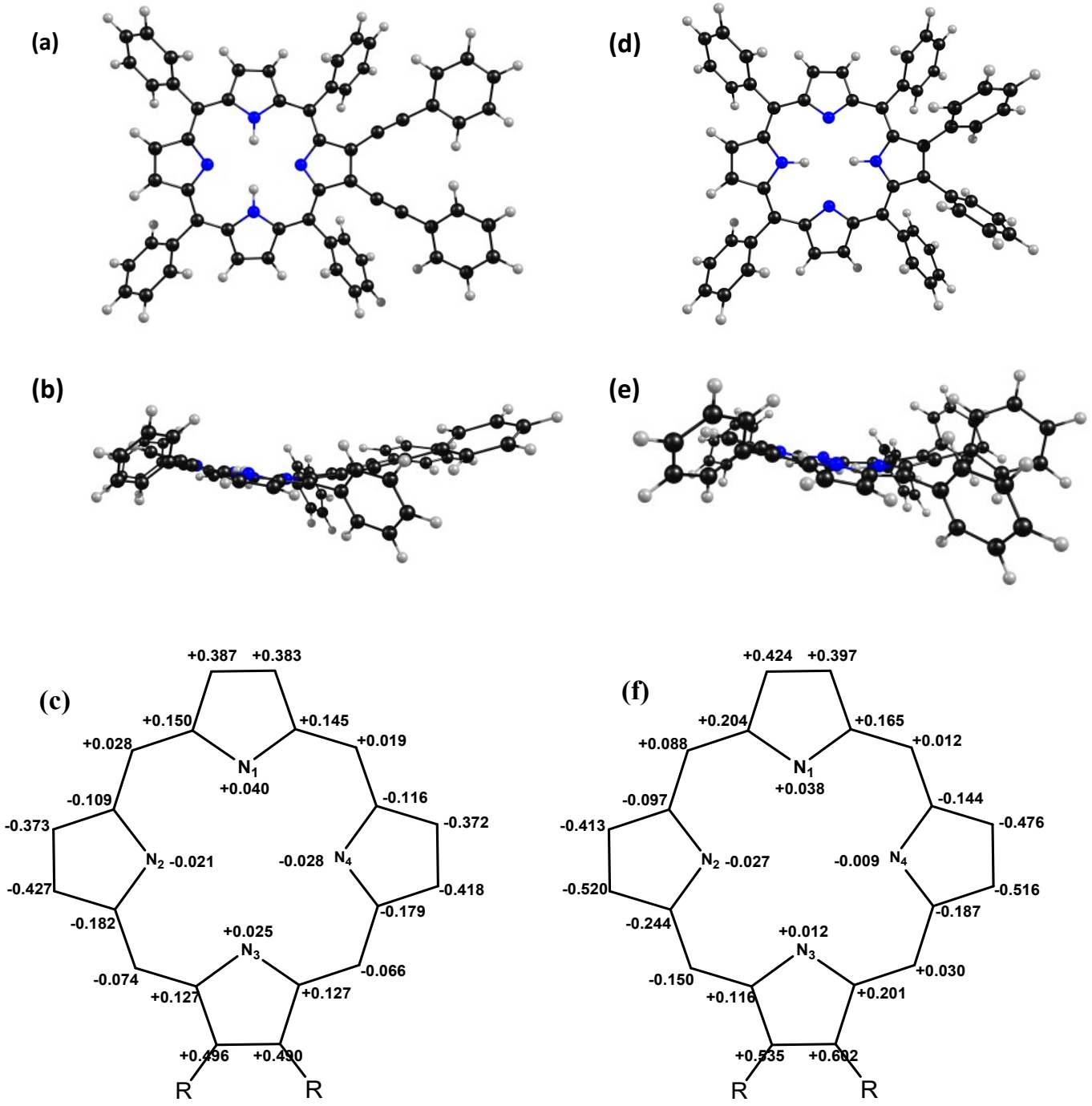

Figure S1. B3LYP/6-31G optimized geometries showing top as well as side views of $H_2TPP(PE)_2$ (**1a** and **1b**) and $H_2TPP(Ph)_2$ (**1d** and **1e**), respectively. The displacement of porphyrin-core atoms in Å from the mean plane are shown in figures **1c** and **1f** for $H_2TPP(PE)_2$ and $H_2TPP(Ph)_2$, respectively. Color codes for atoms: C (black), N (blue) and H (white).

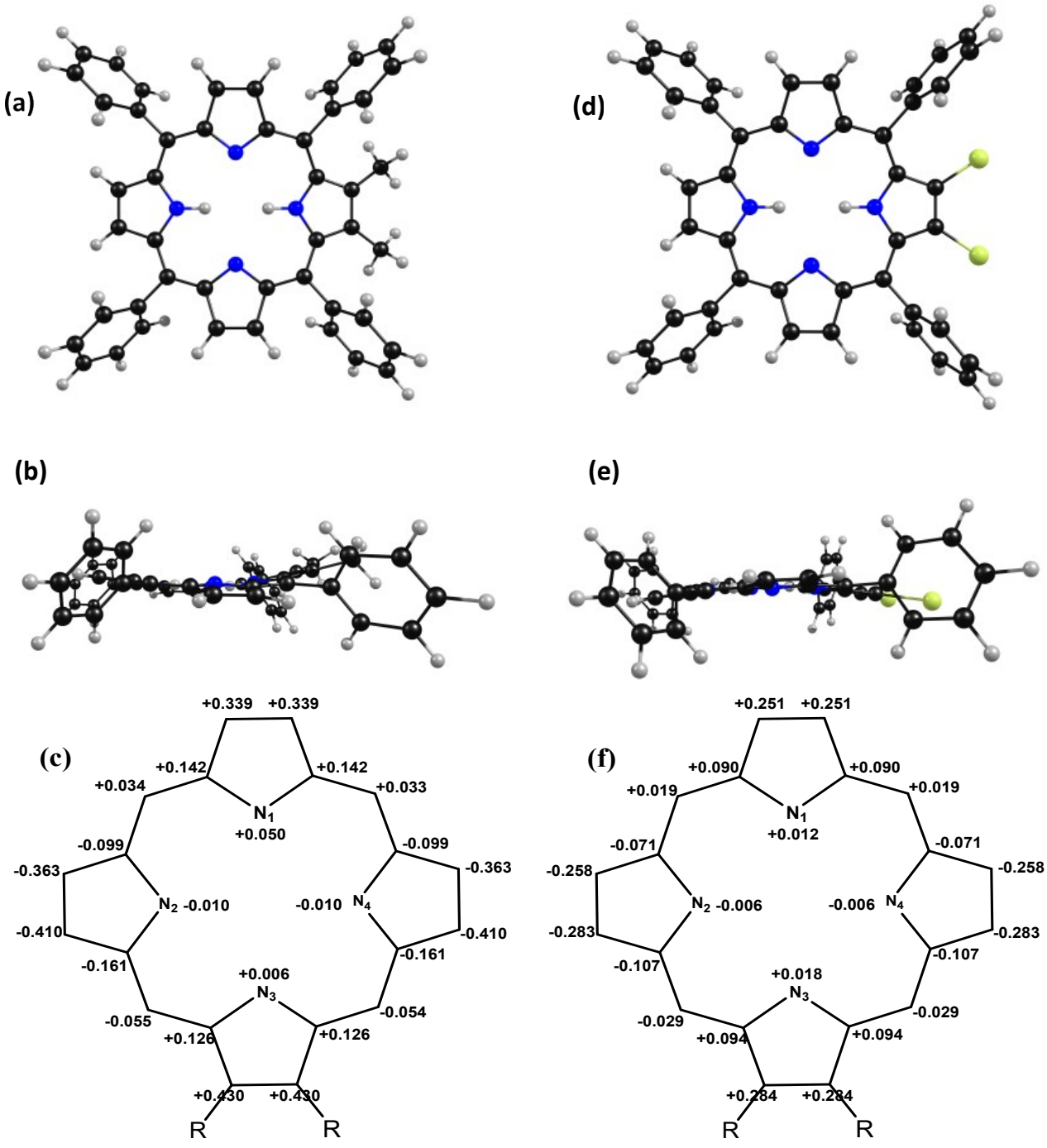

Figure S2. B3LYP/6-31G optimized geometries showing top as well as side views of $H_2TPP(CH_3)_2$ (**1a** and **1b**) and $H_2TPP(Br)_2$ (**1d** and **1e**), respectively. The displacement of porphyrin-core atoms in Å from the mean plane are shown in figures **1c** and **1f** for $H_2TPP(CH_3)_2$ and $H_2TPP(Br)_2$, respectively. Color codes for atoms: C (black), N (blue), H (white) and Br (parrot-green).

Table S3. Selected bond lengths (Å), bond angles (º) and calculated dipole moment for the B3LYP/6-31G optimised geometries of $H_2TPP(X)_2$ (X = PE, CH_3, Ph and Br).

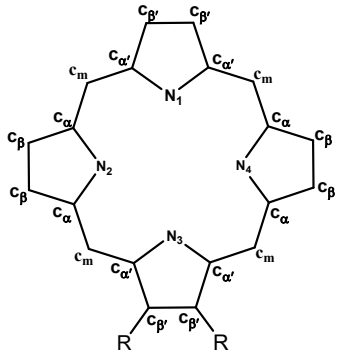

R = CH_3, PE, Ph & Br

	$H_2TPP(PE)_2$	$H_2TPP(CH_3)_2$	$H_2TPP(Ph)_2$	$H_2TPP(Br)_2$
Bond Length (Å)				
N-C_α	1.386	1.383	1.382	1.384
N′-C_α	1.381	1.385	1.386	1.387
C_α-C_β	1.439	1.464	1.464	1.465
$C_{\alpha'}$-$C_{\beta'}$	1.467	1.446	1.445	1.439
C_β-C_β	1.373	1.359	1.357	1.358
$C_{\beta'}$-$C_{\beta'}$	1.379	1.382	1.385	1.375
C_α-C_m	1.406	1.413	1.412	1.411
$C_{\alpha'}$-C_m	1.413	1.407	1.408	1.406
ΔC_β (Å)[a]	0.418	0.386	0.485	0.269
Δ24 (Å)[b]	0.199	0.183	0.236	0.125
Bond Angle (deg)				
N-C_α-C_m	127.14	126.65	126.32	126.88
N′-$C_{\alpha'}$-C_m	125.33	125.39	125.47	125.85
N-C_α-C_β	106.25	110.27	110.25	110.39
N′-$C_{\alpha'}$-$C_{\beta'}$	110.15	106.41	106.36	106.03
C_β- C_α-C_m	126.58	123.06	123.41	123.47
$C_{\beta'}$- $C_{\alpha'}$-C_m	124.76	128.27	128.12	128.36
C_α-C_m-$C_{\alpha'}$	124.92	125.25	124.78	125.22
C_α-C_β-C_β	108.39	106.82	106.82	106.79
$C_{\alpha'}$-$C_{\beta'}$-$C_{\beta'}$	106.51	108.12	108.09	108.56
C_α-N-C_α	110.68	105.76	106.31	106.11
$C_{\alpha'}$-N- $C_{\alpha'}$	107.05	110.86	110.96	111.27
Dipole moment	0.884D		0.467D	2.956D

[a]ΔC_β refers to the mean plane displacement of the β-pyrrole carbons

[b]Δ24 refers to the mean plane deviation of 24-atom core

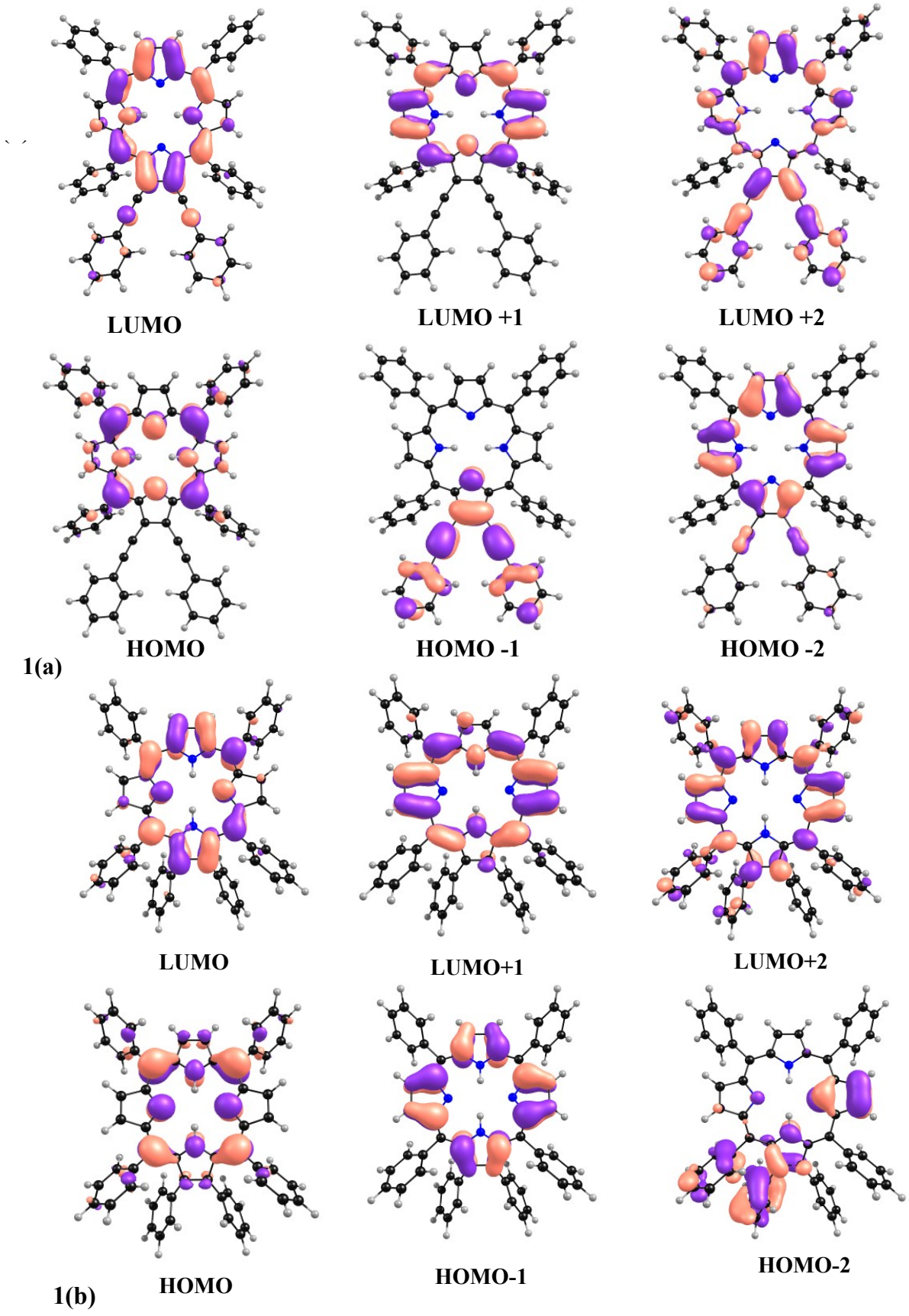

Figure S3. B3LYP/6-31G optimised geometries showing Frontier Molecular Orbitals (FMOs) of $H_2TPP(PE)_2$ (1a) and $H_2TPP(Ph)_2$ (1b), respectively (having isosurface contour value of 0.03)

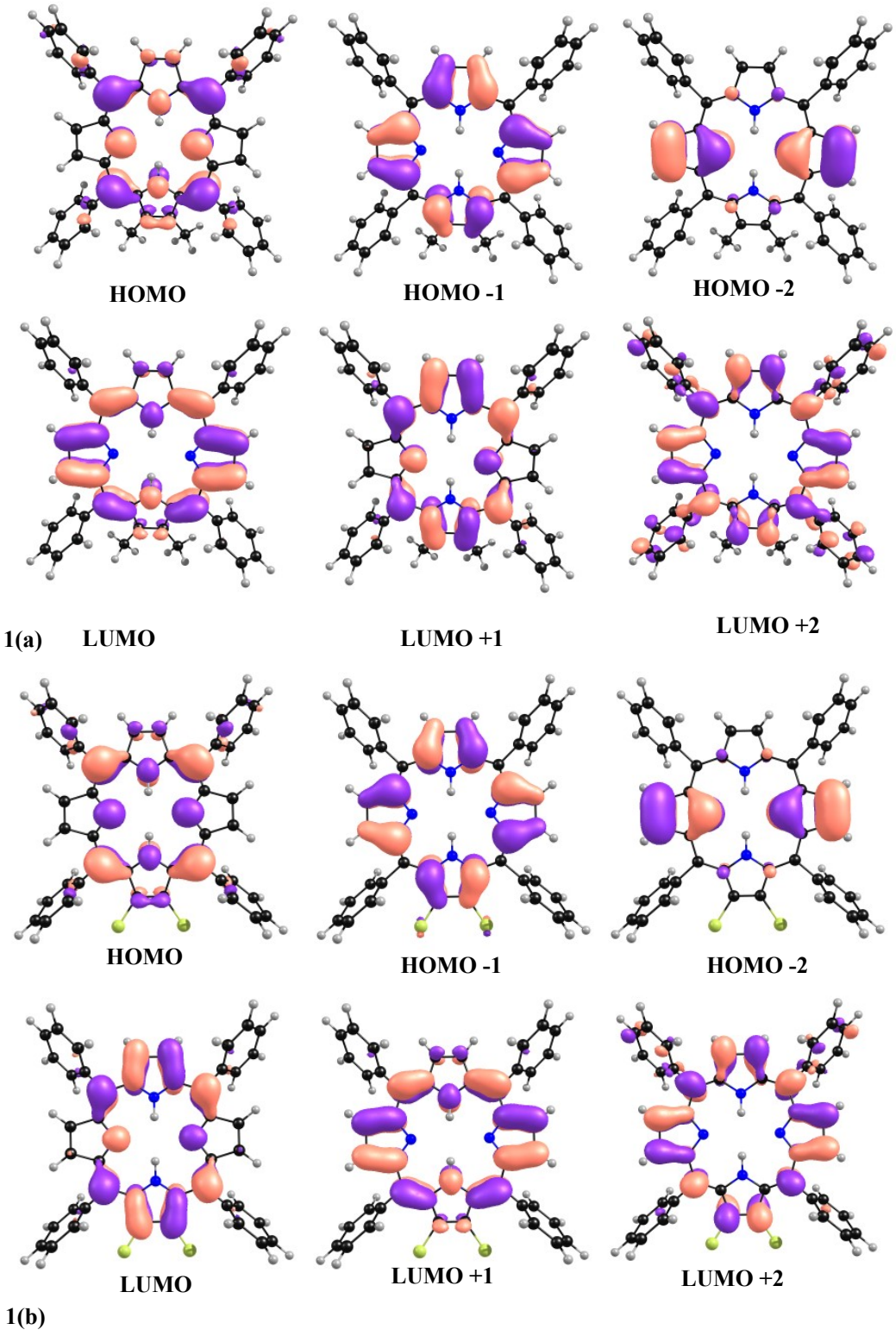

Figure S4. B3LYP/6-31G optimized geometries showing Frontier Molecular Orbitals (FMOs) of $H_2TPP(CH_3)_2$ (1a) and $H_2TPP(Br)_2$ (1b), respectively (having isosurface contour value of 0.03).

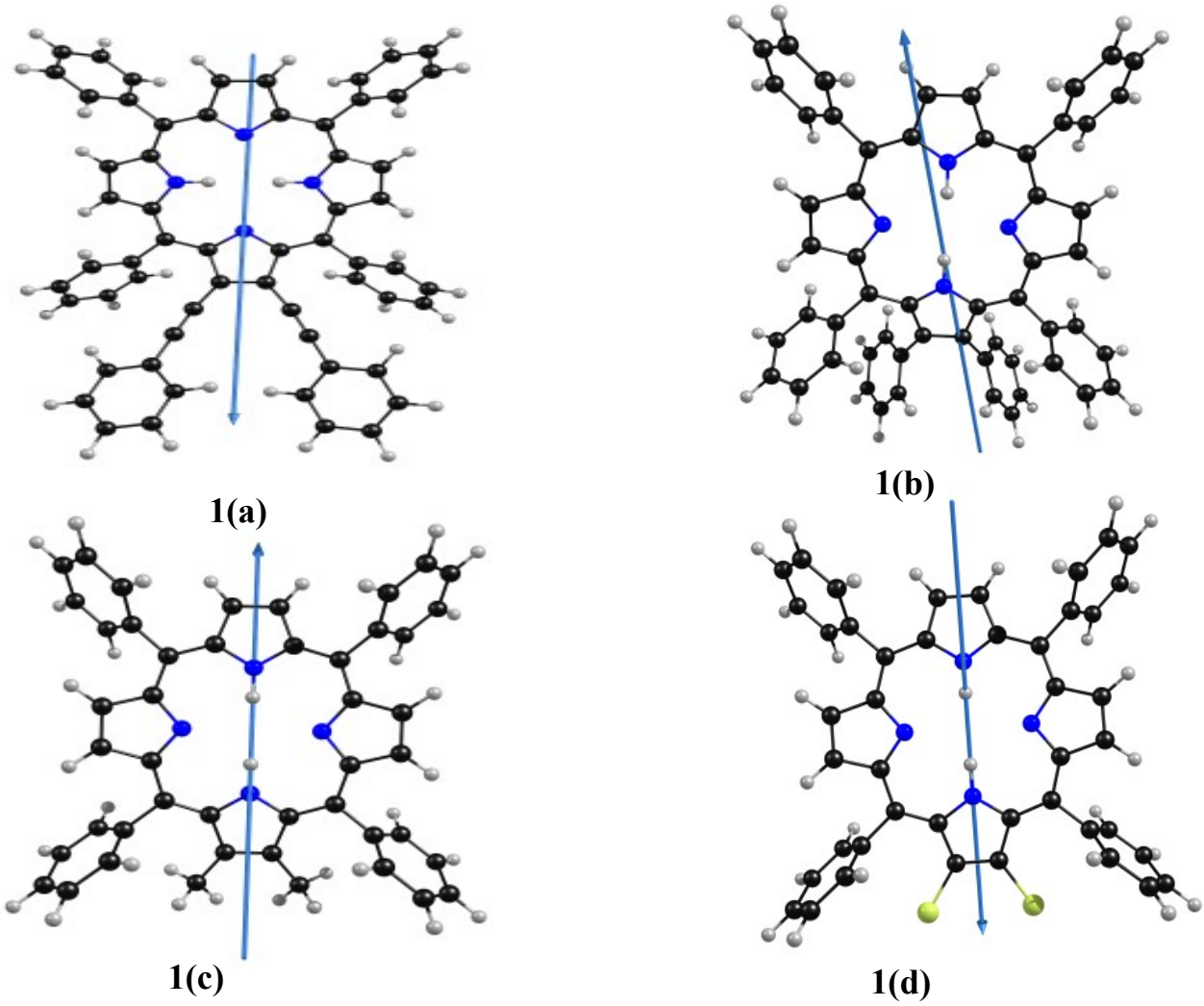

Figure S5. B3LYP/6-31G optimized geometries showing direction of dipole moment of $H_2TPP(PE)_2$ (1a), $H_2TPP(Ph)_2$ (1b), $H_2TPP(CH_3)_2$ (1c) and $H_2TPP(Br)_2$ (1d), respectively.

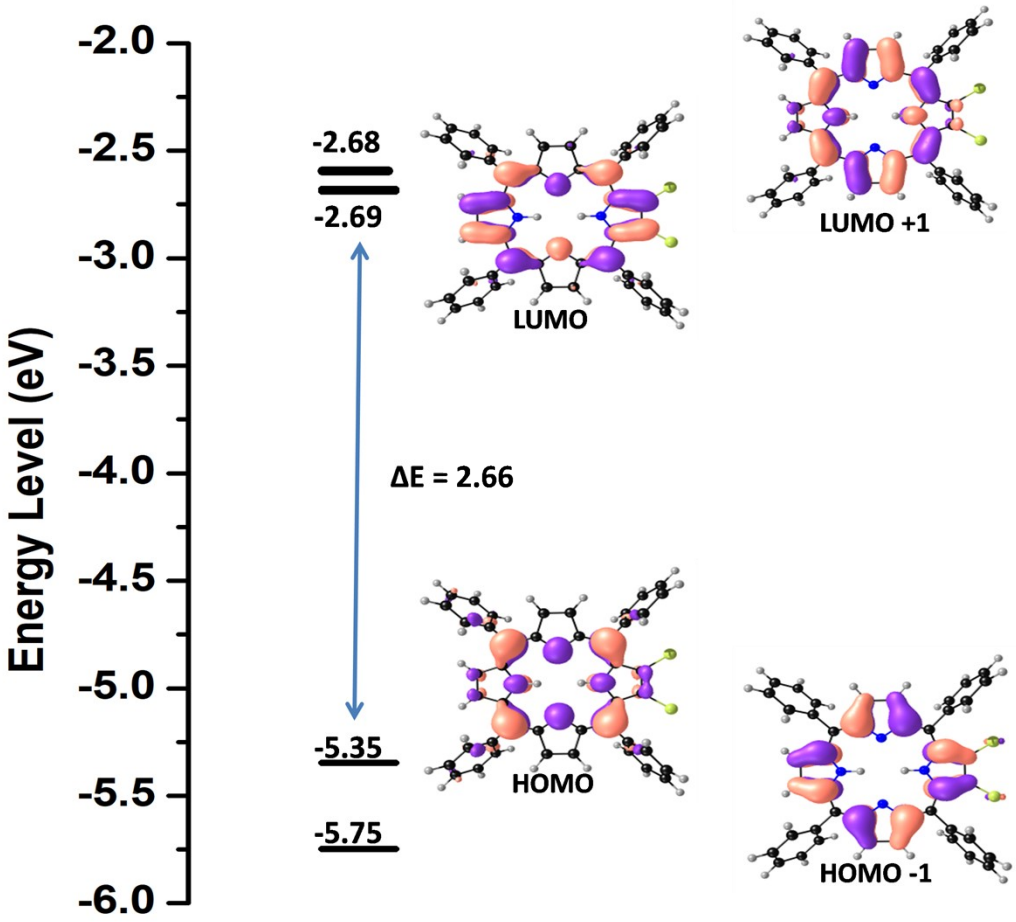

Figure S6. Molecular orbital energy level diagrams of $H_2TPP(Br)_2$ obtained at the B3LYP/6-31G basis set (Gaussian 16 package).

Table S4. Optical absorption spectral data of all the newly synthesized regioselective *β*-disubstituted free base porphyrins as well as their metal complexes. Values in parentheses refer to log ε (ε in Mol^{-1} cm^{-1}).

Porphyrins	Soret band, (nm)	Q band(s), (nm)
$H_2TPP(Br)_2$	424 (5.19)	521 (4.22), 560 (sh), 598 (3.71), 656 (3.78)
$H_2TPP(PE)_2$	438 (5.46)	529 (4.35), 567 (3.96), 610 (3.87), 668 (3.76)
$H_2TPP(Ph)_2$	424 (5.53)	519 (4.27), 555 (3.84), 595 (3.78), 653 (3.53)
$H_2TPP(CH_3)_2$	419 (5.50)	516 (3.65), 588 (3.65), 643 (3.72)
$CuTPP(Br)_2$	420 (5.58)	544 (4.33)
$CuTPP(PE)_2$	437 (5.50)	557 (3.86), 598 (3.60)
$CuTPP(Ph)_2$	420 (5.50)	544 (4.20)
$CuTPP(CH_3)_2$	416 (5.36)	541 (3.25)
$CoTPP(Br)_2$	417 (5.58)	538 (4.42)
$CoTPP(PE)_2$	433 (5.37)	549 (3.40), 589 (3.44)
$CoTPP(Ph)_2$	416 (5.34)	537 (4.19)
$CoTPP(CH_3)_2$	411 (5.37)	533 (4.45)
$NiTPP(Br)_2$	422 (5.47)	538 (4.30)
$NiTPP(PE)_2$	438 (5.54)	548 (4.41), 593 (4.38)
$NiTPP(Ph)_2$	422 (5.36)	538 (4.18)
$NiTPP(CH_3)_2$	417 (5.32)	534 (3.38)
$ZnTPP(Br)_2$	424 (5.48)	553 (4.28)
$ZnTPP(PE)_2$	442 (5.61)	565 (4.15), 607 (3.91)
$ZnTPP(Ph)_2$	423 (5.57)	552 (4.22),
$ZnTPP(CH_3)_2$	418(5.43)	548 (3.88)

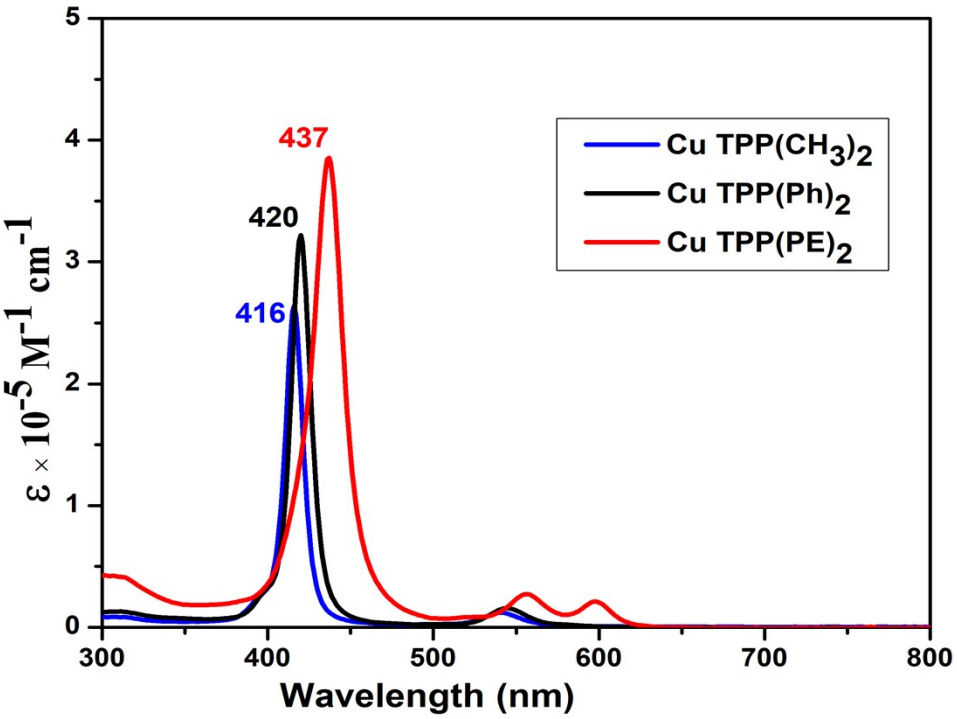

Figure S7. UV- Visible spectra of $CuTPP(X)_2$ (X = CH_3, Ph, PE) derivatives in CH_2Cl_2.

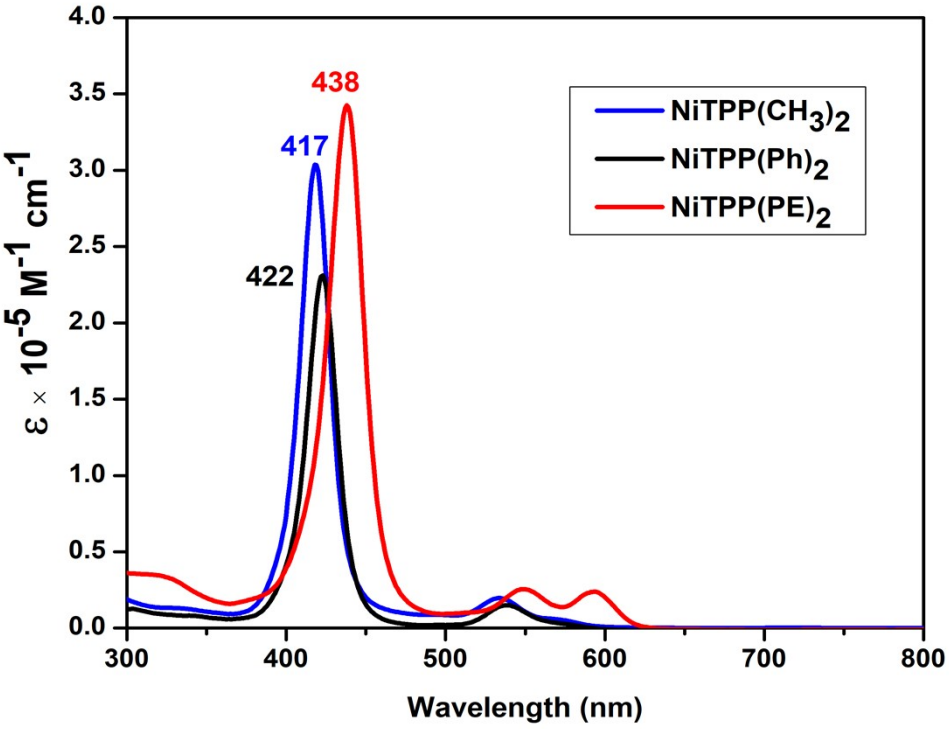

Figure S8. UV- Visible spectra of $NiTPP(X)_2$ (X = CH_3, Ph, PE) derivatives in CH_2Cl_2.

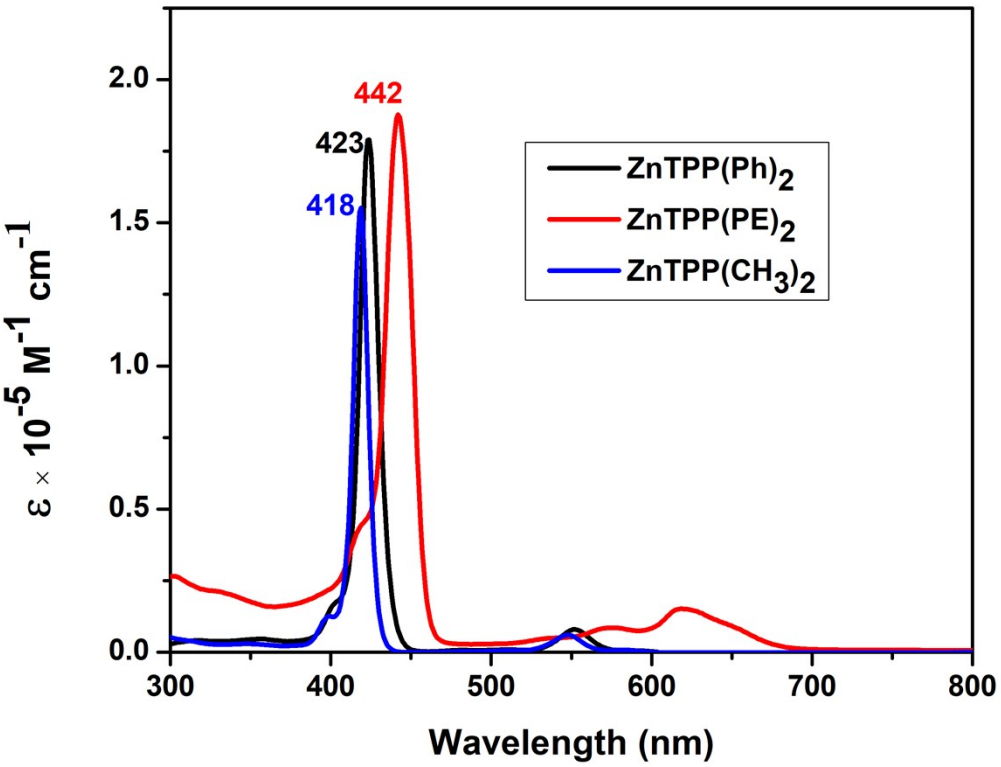

Figure S9. UV- Visible spectra of $ZnTPP(X)_2$ (X = CH_3, Ph, PE) derivatives in CH_2Cl_2.

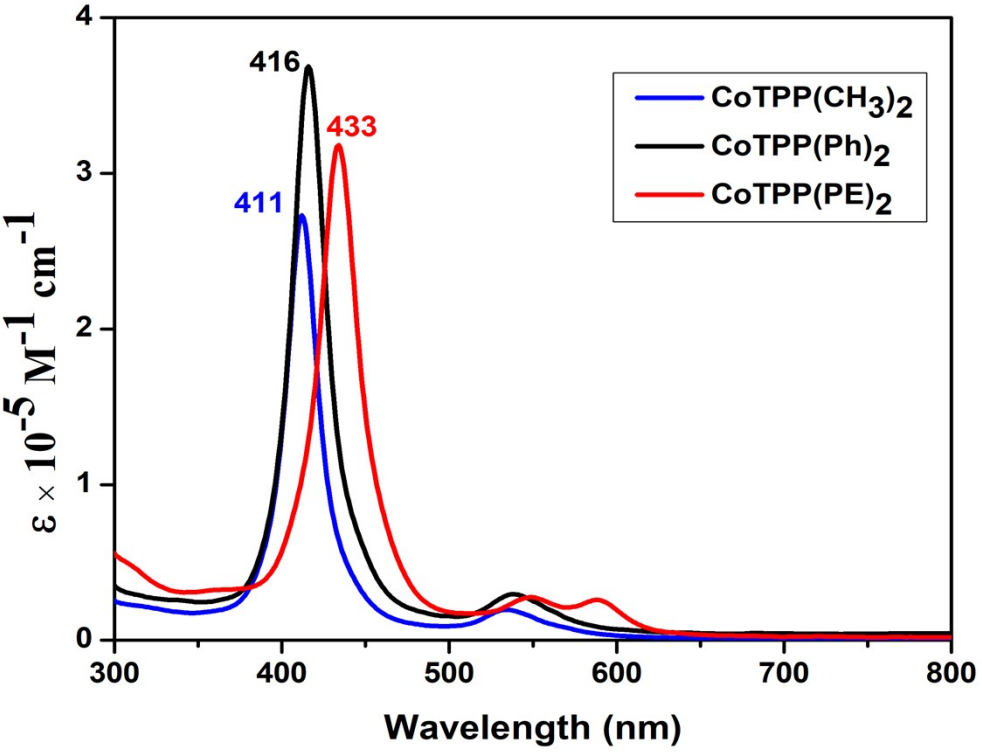

Figure S10. UV- Visible spectra of $CoTPP(X)_2$ (X = CH_3, Ph, PE) derivatives in CH_2Cl_2.

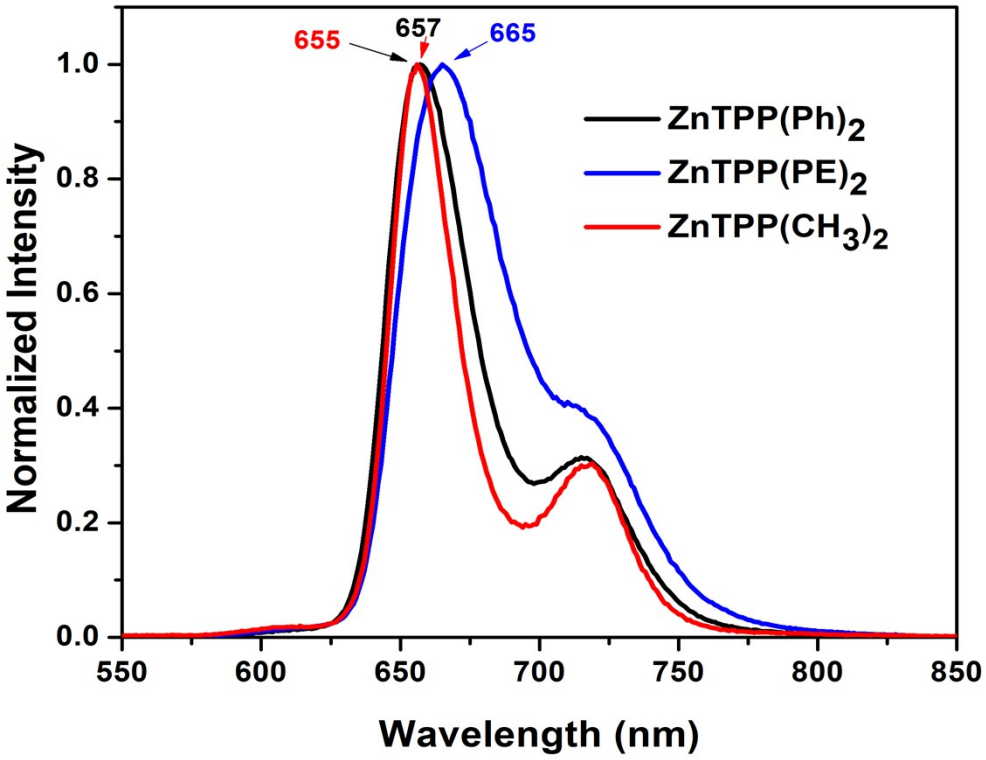

Figure S11. Fluorescence spectra of $ZnTPP(X)_2$ (X = CH_3, Ph, PE) derivatives in CH_2Cl_2 at 298 K.

Table S5. Fluorescence spectral data of $ZnTPP(X)_2$ (X = Br, CH_3, Ph, PE) derivatives in CH_2Cl_2 at 298 K, (Φ_f = quantum yield relative to those of ZnTPP in DCM).

Porphyrins	**λ excitation, nm**	**λ emission, nm**	**Φ_f**
$ZnTPP(Br)_2$	424	652	0.0012
$ZnTPP(CH_3)_2$	418	655	0.0152
$ZnTPP(Ph)_2$	423	657	0.0136
$ZnTPP(PE)_2$	442	665	0.0281

Table S6. Electrochemical redox data of regioselective *β*-disubstituted porphyrins and their metal complexes $MTPP(X)_2$ [M = H_2, Cu(II), Ni(II) & Zn(II), X = CH_3, Ph, PE & Br] in CH_2Cl_2 containing 0.1 M $TBAPF_6$ with a scan rate of 0.1 V/s at 298 K.

Porphyrins	Oxidation (V)			Reduction (V)			ΔE (V)
	I-Oxd	II-Oxd	III-Oxd	I-Red	II-Red	III-Red	
$H_2TPP(PE)_2$	1.05	1.27		-0.99	-1.23		2.04
$CuTPP(PE)_2$	1.00	1.39		-1.17	-1.49		2.17
$CoTPP(PE)_2$	0.89	1.12	1.31	-0.72	-1.16	-1.49	2.28
$NiTPP(PE)_2$	1.08	1.35	1.84	-1.11	-1.39		2.19
$ZnTPP(PE)_2$	0.88	1.13		-1.22	-1.50		2.10
$H_2TPP(Br)_2$	1.07	1.26		-1.01	-1.19		2.08
$CuTPP(Br)_2$	1.02	1.42		-1.16	-1.48		2.18
$CoTPP(Br)_2$	0.93	1.14	1.33	-0.72	-1.23		2.37
$NiTPP(Br)_2$	1.13	1.34		-1.14	-1.39		2.27
$ZnTPP(Br)_2$	0.91	1.15		-1.31	-1.50		2.22
$H_2TPP(Ph)_2$	0.93	1.12		-1.21	-1.36		2.14
$CuTPP(Ph)_2$	0.85	1.26		-1.32	-1.60		2.17
$CoTPP(Ph)_2$	0.95	1.17	1.56	-0.83	-1.21		2.38
$NiTPP(Ph)_2$	0.98	1.31	1.86	-1.24			2.22
$ZnTPP(Ph)_2$	0.87	1.07		-1.38	-1.48		2.25
$H_2TPP(CH_3)_2$	0.94	1.15		-1.22	-1.55		2.16
$CuTPP(CH_3)_2$	0.87	1.28		-1.31	-1.51		2.18
$CoTPP(CH_3)_2$	0.83	1.04	1.20	-0.81	-1.05		2.09
$NiTPP(CH_3)_2$	0.96	1.30	1.83	-1.20			2.16
$ZnTPP(CH_3)_2$	0.81	1.01		-1.41	-1.60		2.22

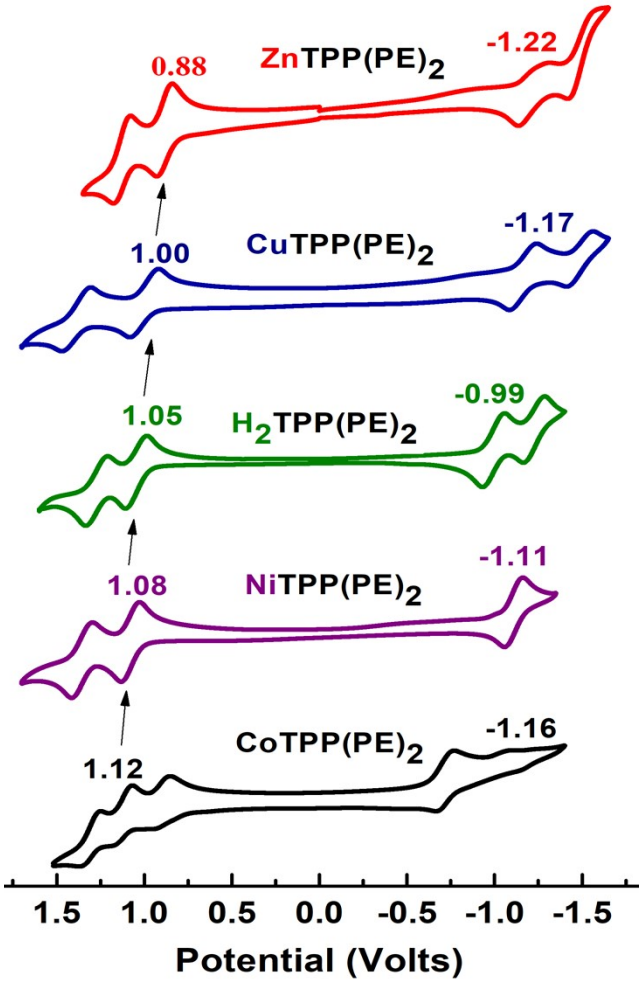

Figure S12. Cyclic voltammograms of $MTPP(PE)_2$ [M= Cu(II), Zn(II), Ni(II) and Co(II)] (~1 mM) in CH_2Cl_2 containing 0.1 M $TBAPF_6$ using Ag/AgCl as reference electrode with a scan rate of 0.10 V/s at 298 K

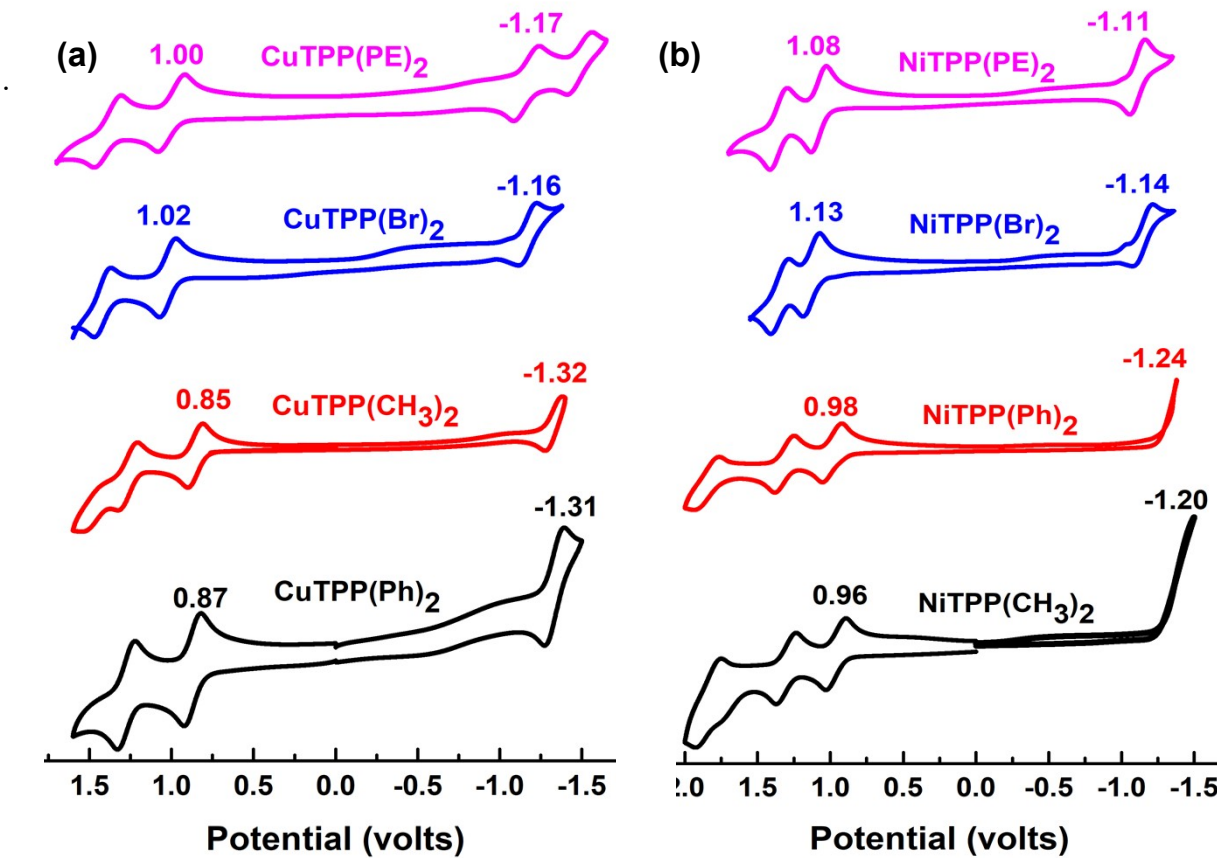

Figure S13. Cyclic voltammograms of (a) $CuTPP(X)_2$ [X= CH_3, Ph, Br and PE] (b) $NiTPP(X)_2$ [X= CH_3, Ph, Br and PE] (~1 mM) in CH_2Cl_2 containing 0.1 M $TBAPF_6$ using Ag/AgCl as reference electrode with a scan rate of 0.10 V/s at 298 K.

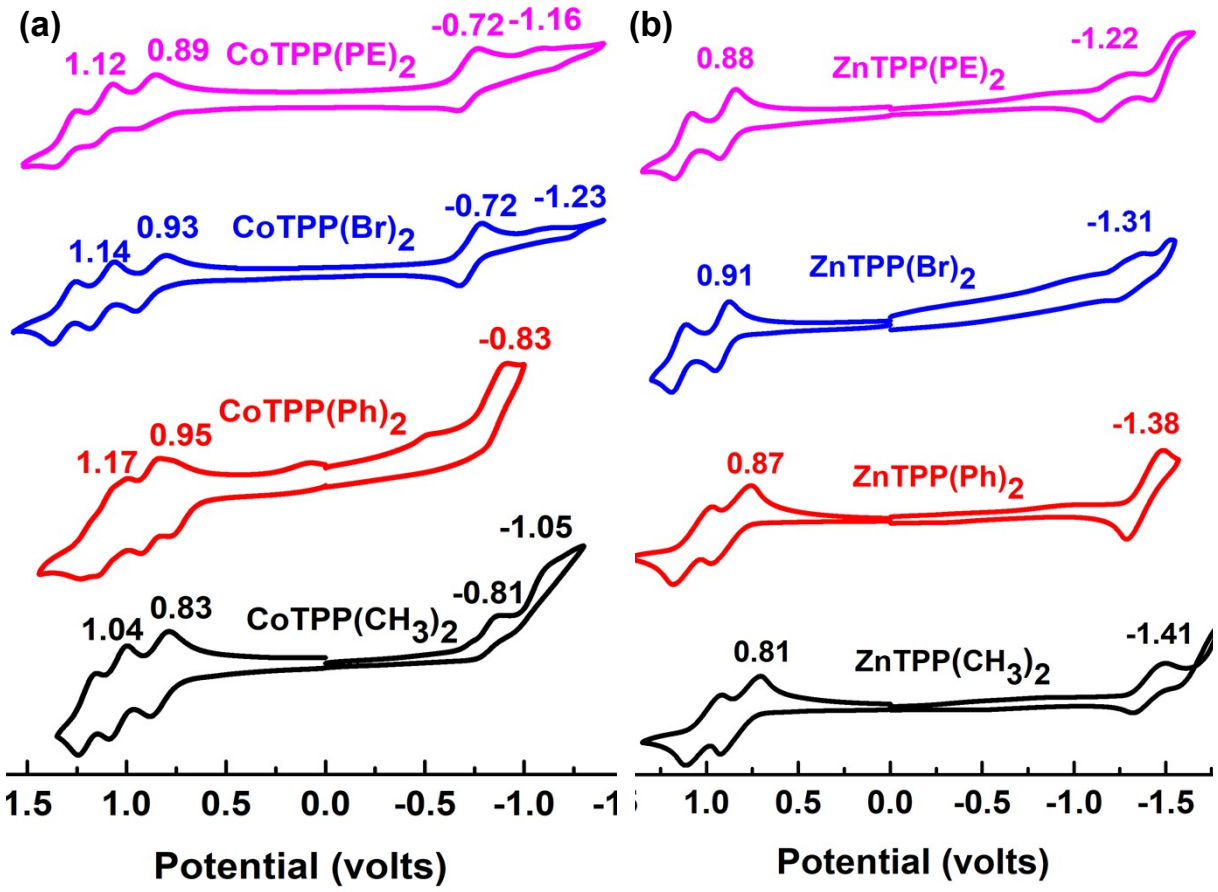

Figure S14. Cyclic voltammograms of (a) $CoTPP(X)_2$ [X= CH_3, Ph, Br and PE] (Zn) $NiTPP(X)_2$ [X= CH_3, Ph, Br and PE] (~1 mM) in CH_2Cl_2 containing 0.1 M $TBAPF_6$ using Ag/AgCl as reference electrode with a scan rate of 0.10 V/s at 298 K.

Figure S15. ^{1}H NMR spectrum of $H_2TPP(Br)_2$ in $CDCl_3$ at 298 K.

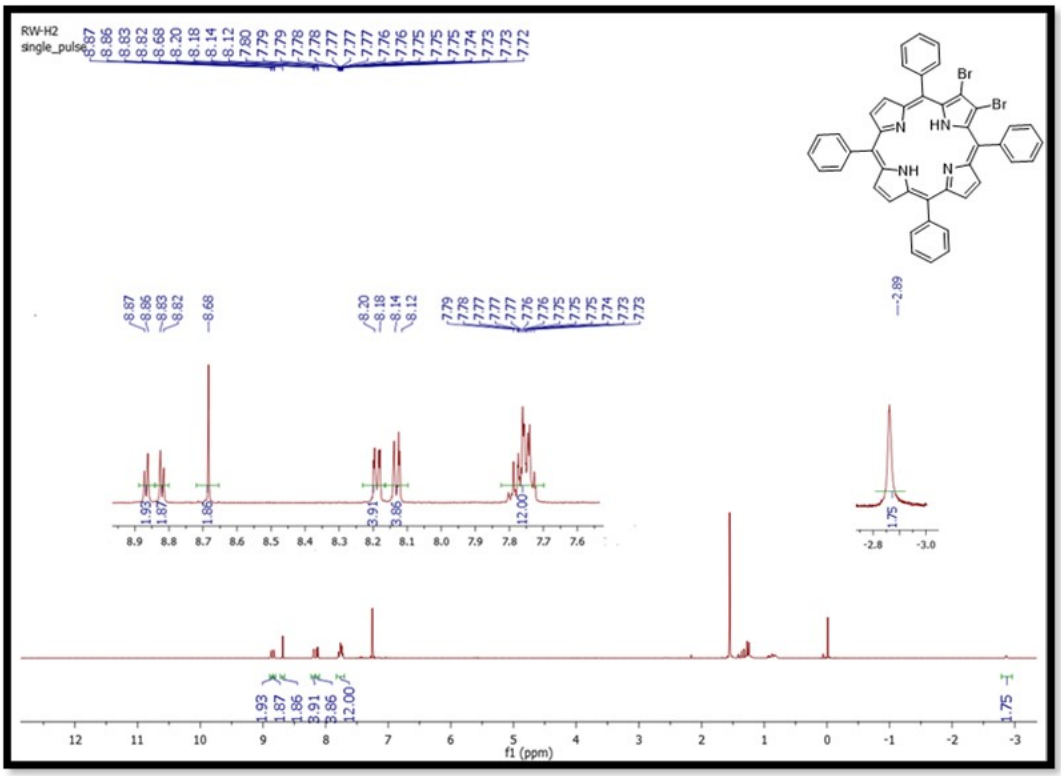

Figure S16. ^{1}H NMR spectrum of $ZnTPP(Br)_2$ in $CDCl_3$ at 298 K.

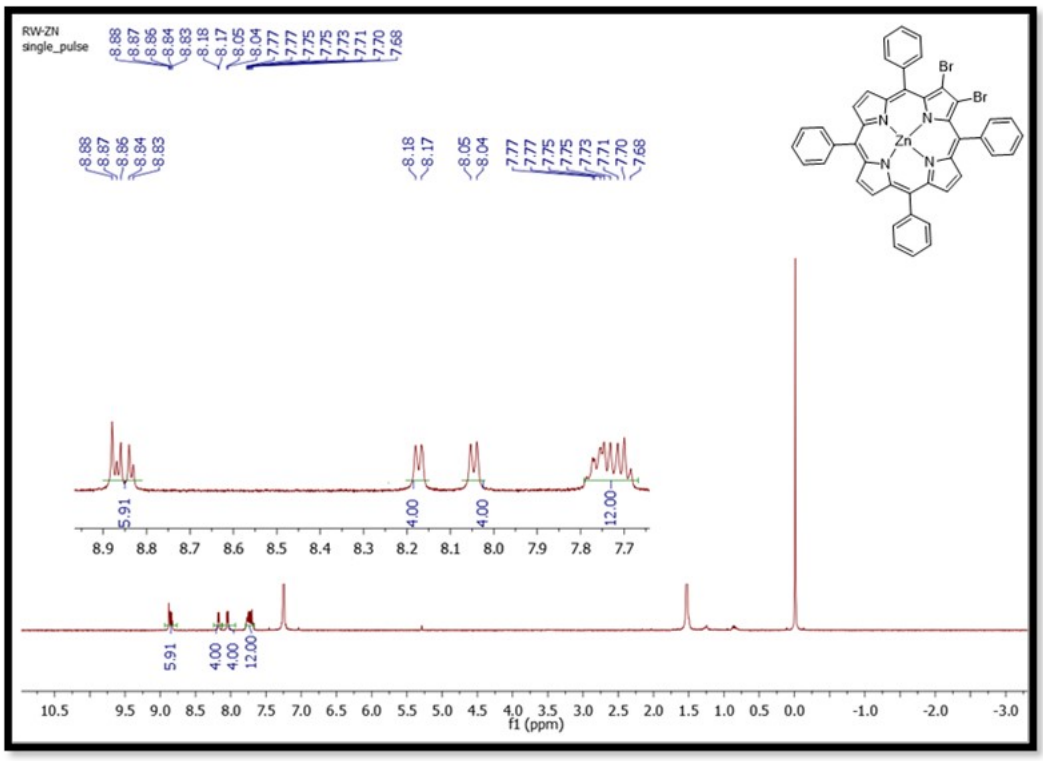

Figure S17. ^{1}H NMR spectrum of $NiTPP(Br)_2$ in $CDCl_3$ at 298 K.

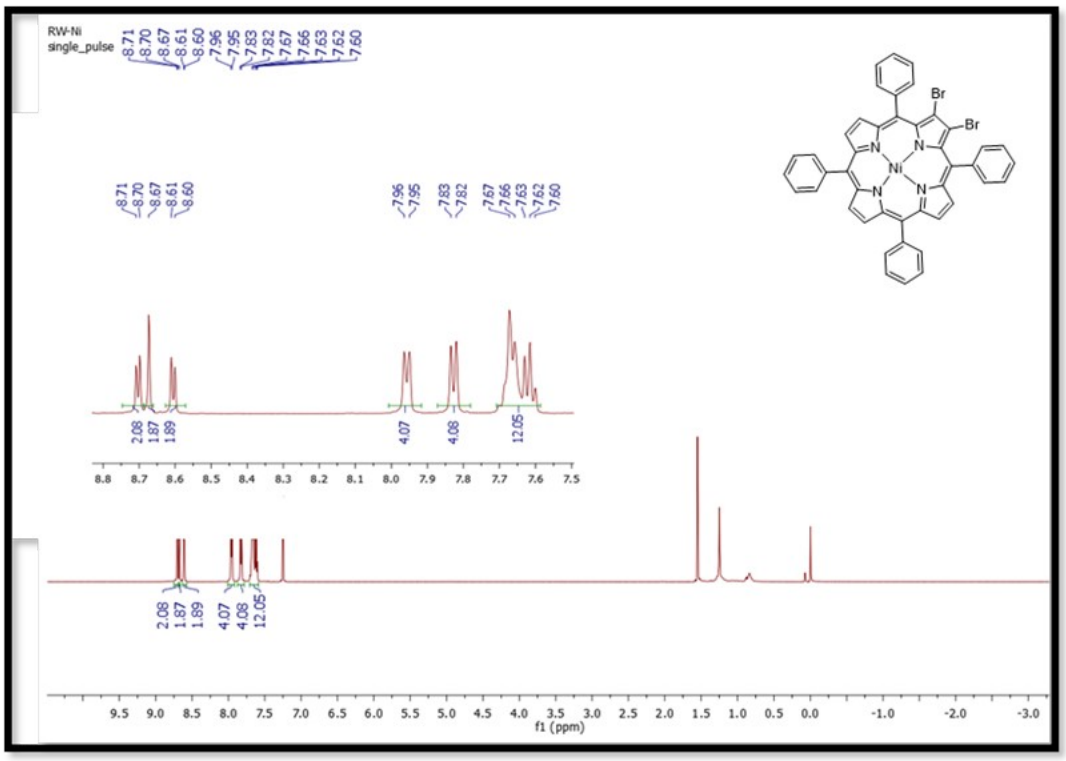

Figure S18. ^{1}H NMR spectrum of $H_2TPP(CH_3)_2$ in $CDCl_3$ at 298 K.

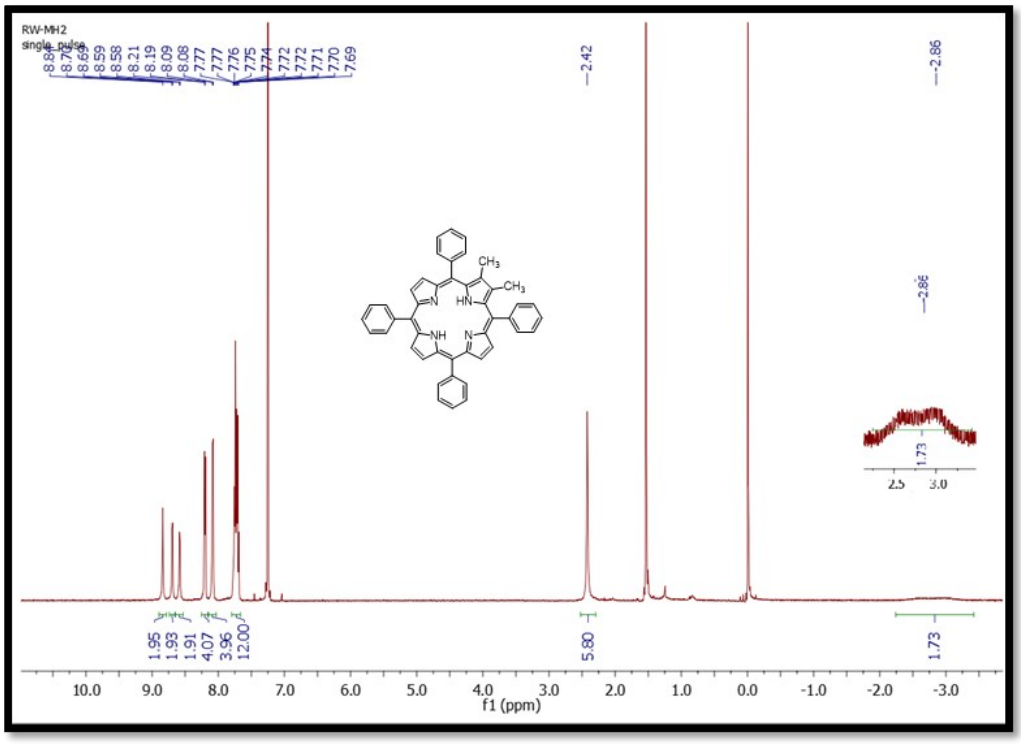

Figure S19. ^{1}H NMR spectrum of NiTPP$(CH_3)_2$ in $CDCl_3$ at 298 K.

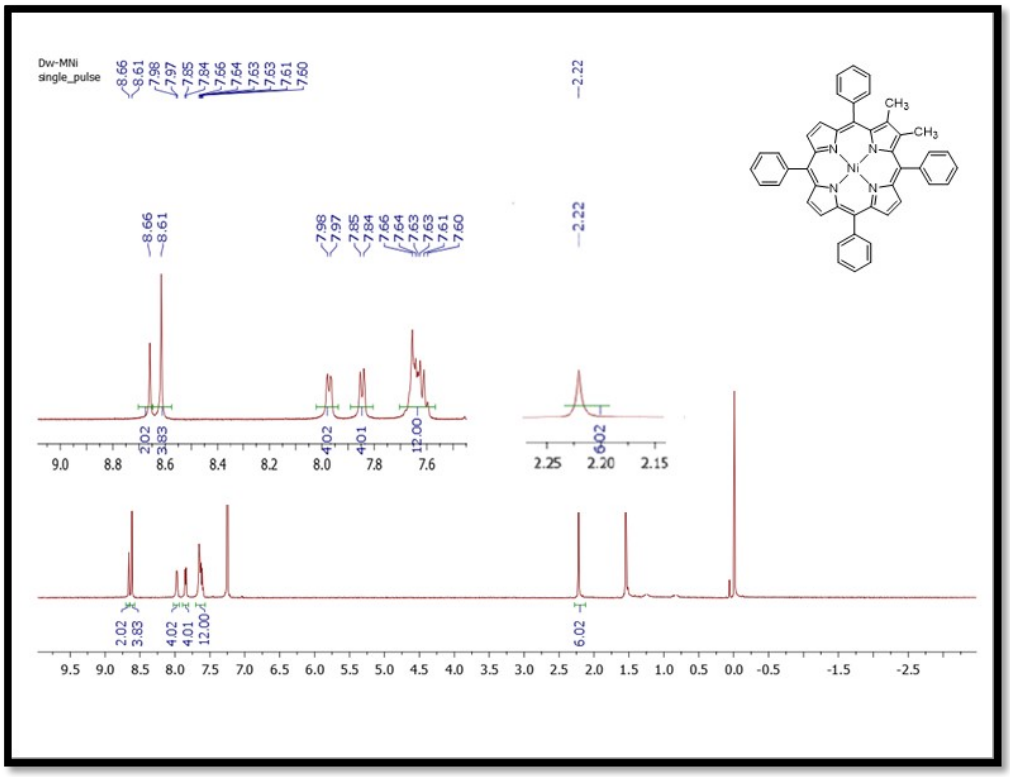

Figure S20. ^{1}H NMR spectrum of ZnTPP$(CH_3)_2$ in $CDCl_3$ at 298 K.

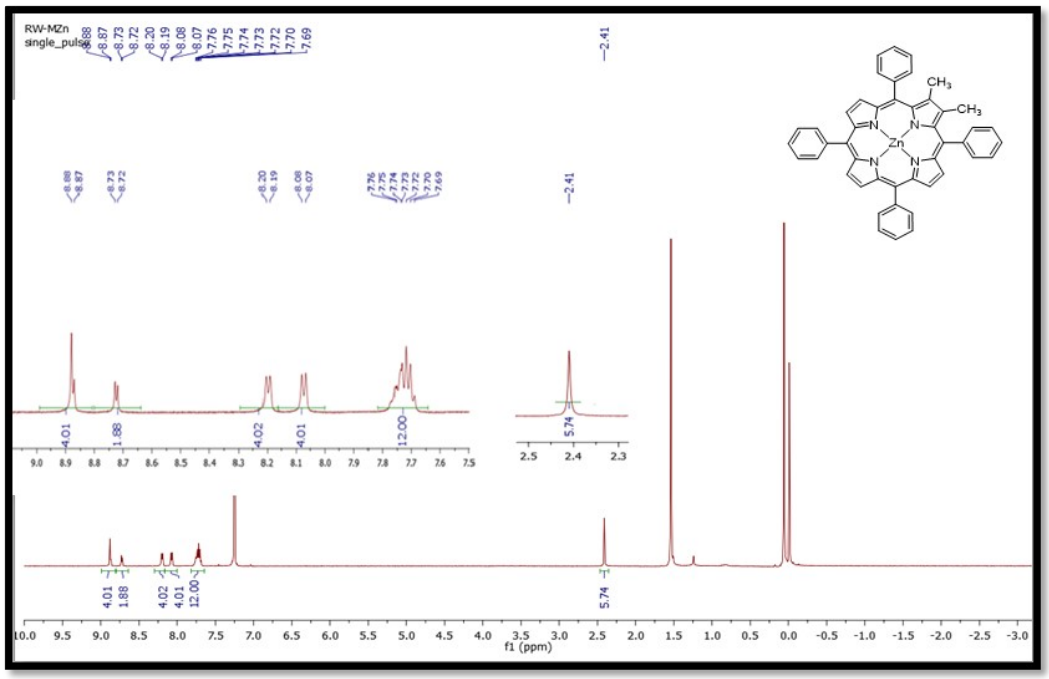

Figure S21. ^{1}H NMR spectrum of $H_2TPP(Ph)_2$ in $CDCl_3$ at 298 K.

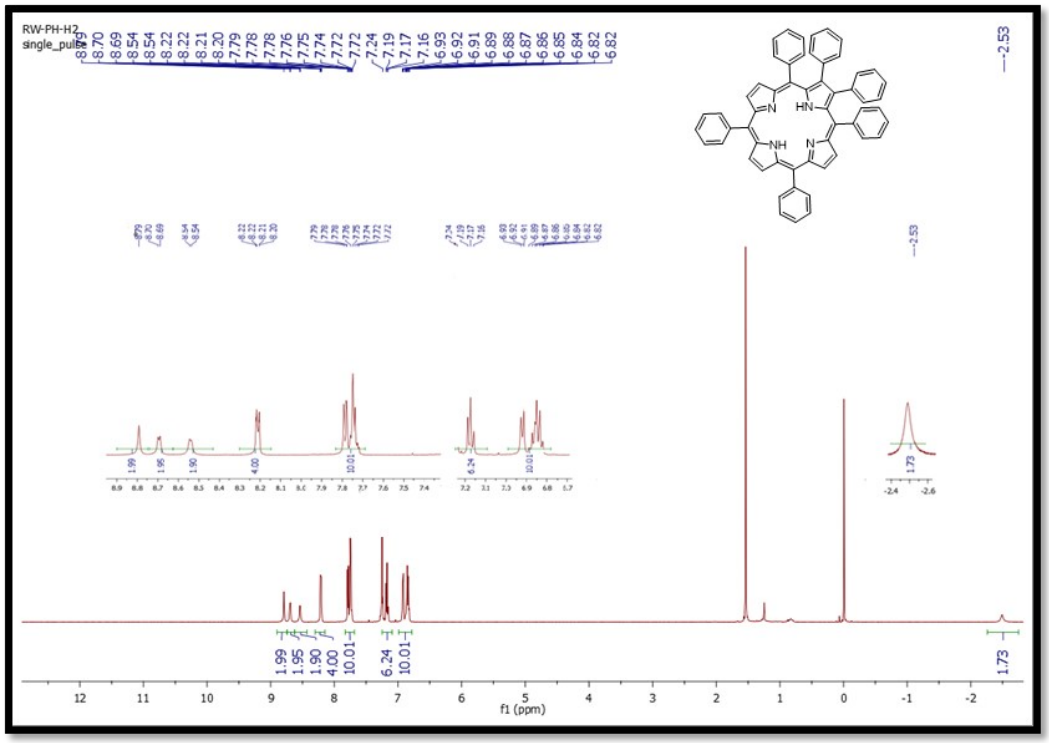

Figure S22. ^{1}H NMR spectrum of $ZnTPP(Ph)_2$ in $CDCl_3$ at 298 K.

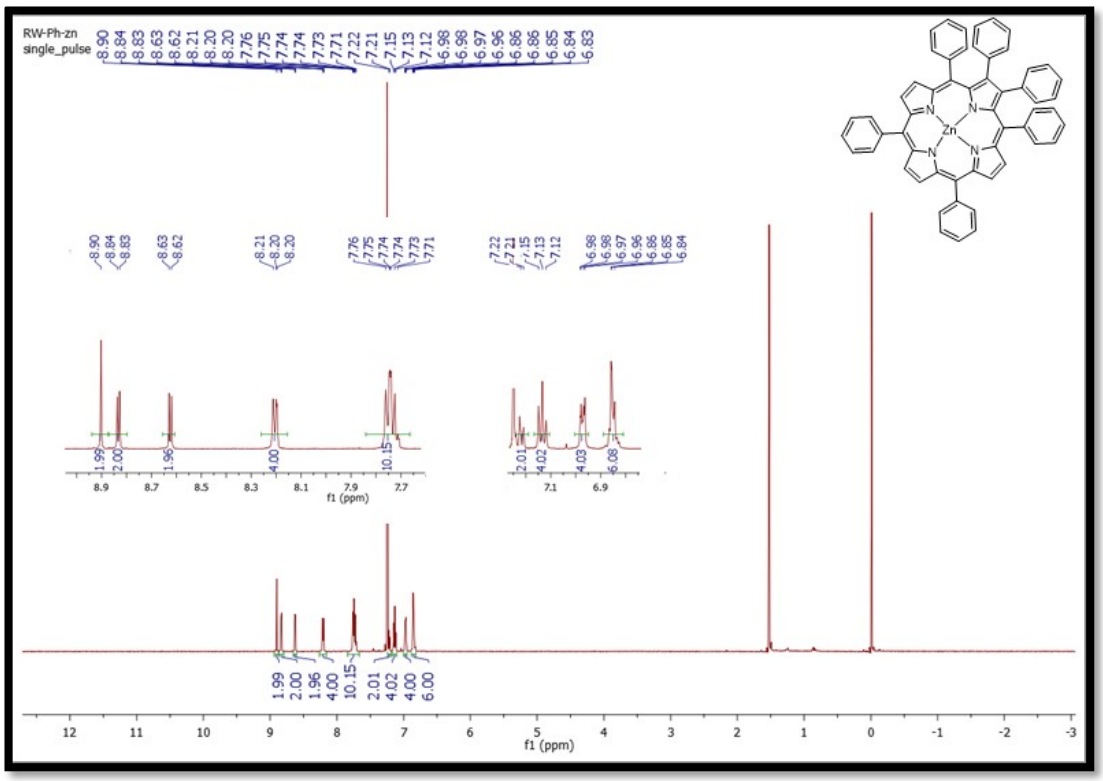

Figure S23. ^{1}H NMR spectrum of NiTPP(Ph)$_2$ in $CDCl_3$ at 298 K.

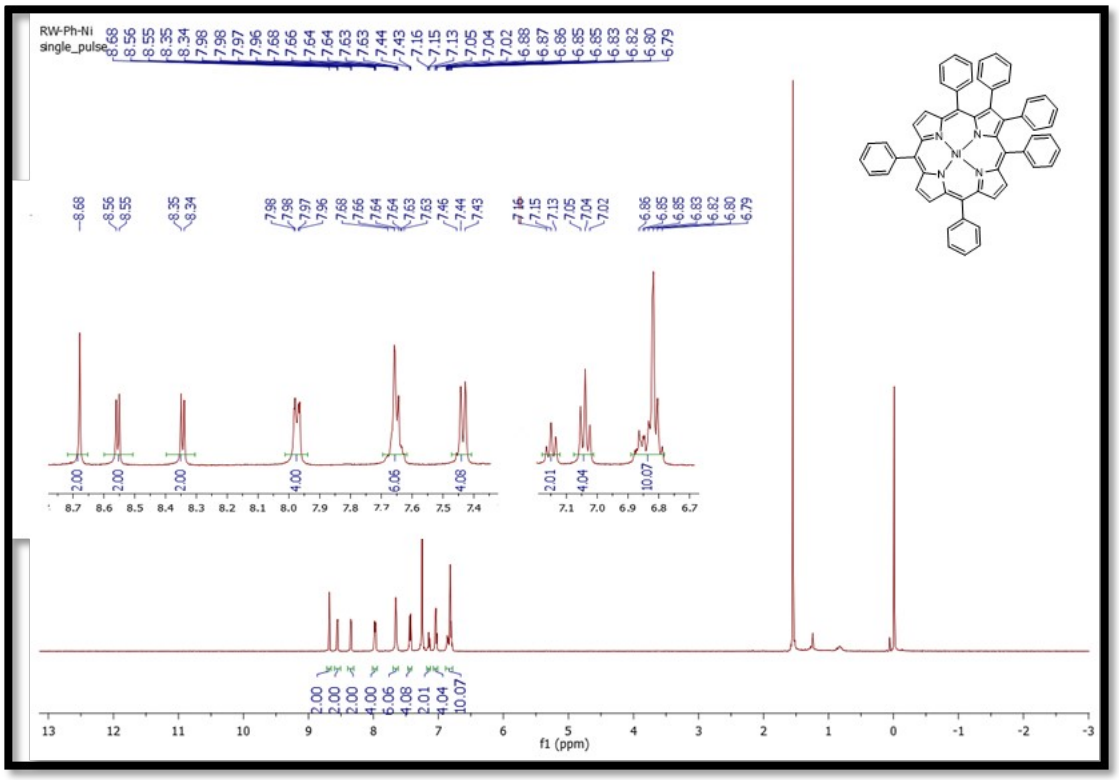

Figure S24. ^{1}H NMR spectrum of H_2TPP(PE)$_2$ in $CDCl_3$ at 298 K.

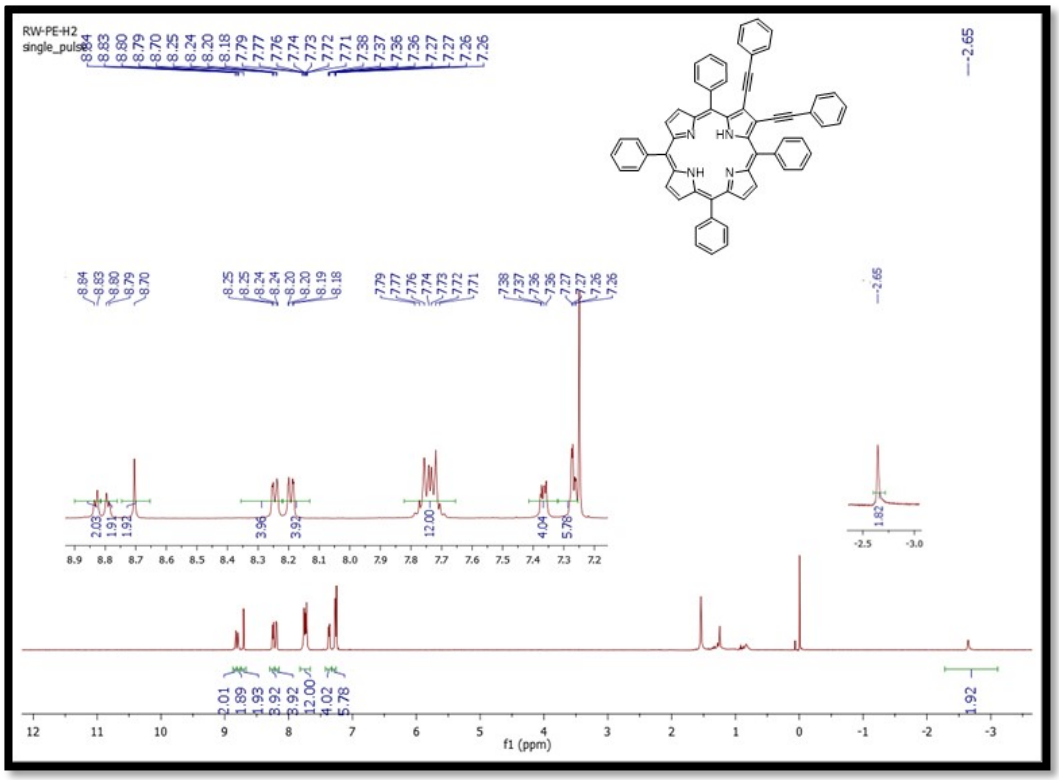

Figure S25. ^{1}H NMR spectrum of ZnTPP(PE)$_2$ in $CDCl_3$ at 298 K.

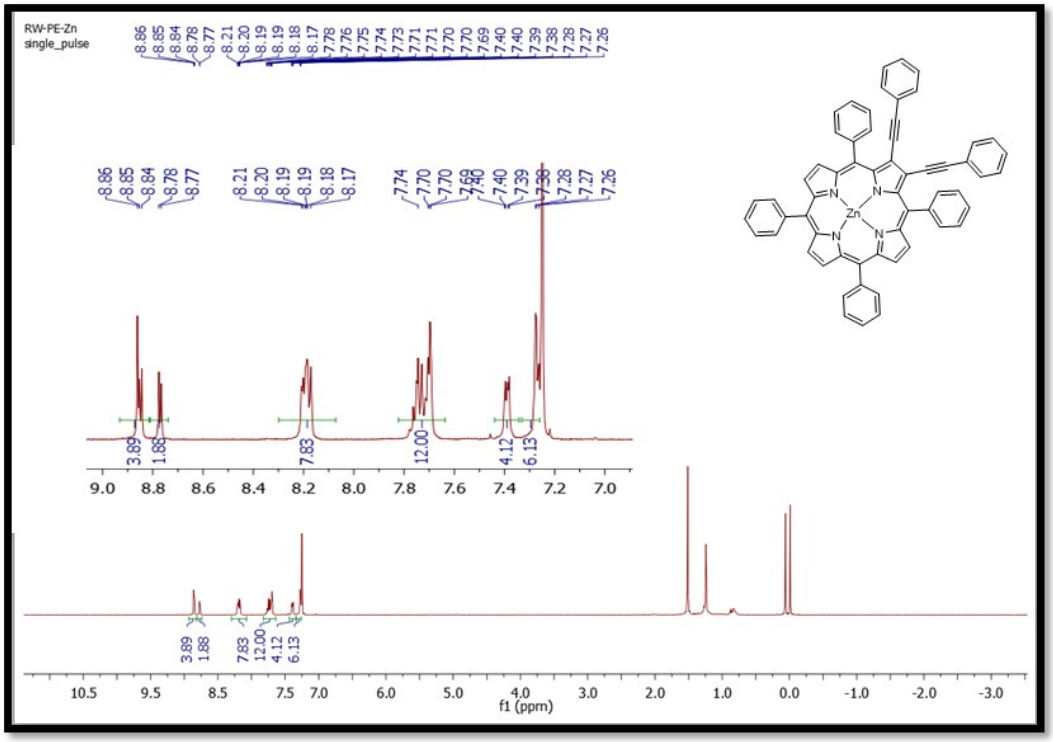

Figure S26. ^{1}H NMR spectrum of NiTPP(PE)$_2$ in $CDCl_3$ at 298 K.

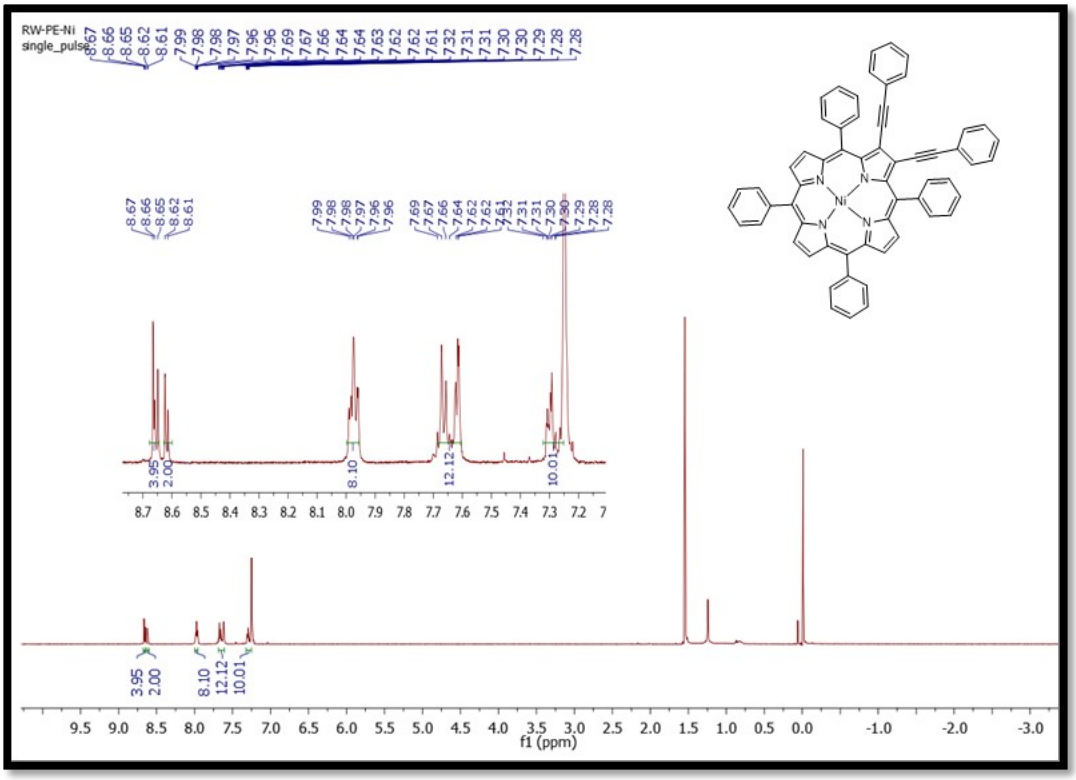

Figure S27. HRMS spectrum of $H_2TPP(Br)_2$.

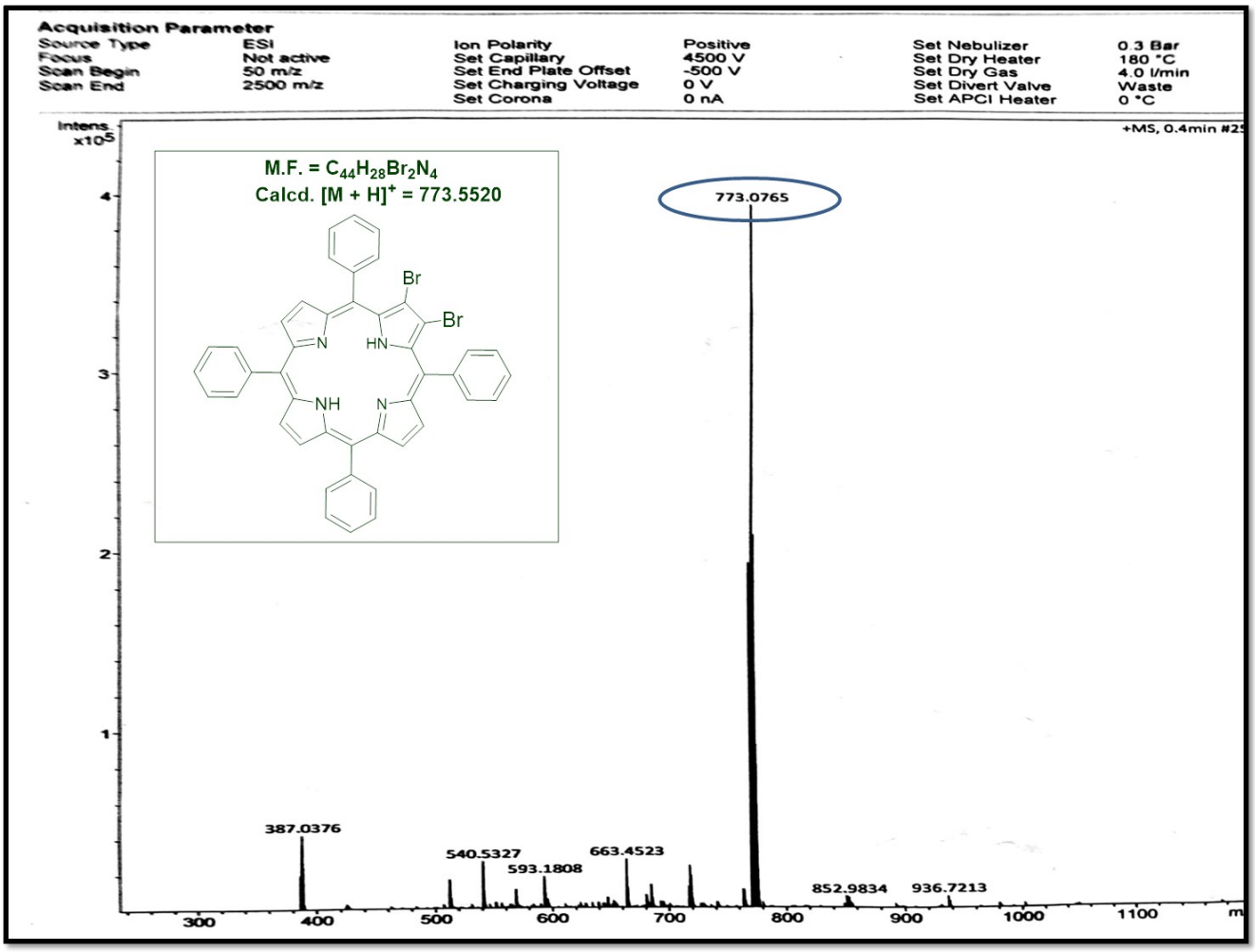

Figure S28. HRMS spectrum of $ZnTPP(Br)_2$.

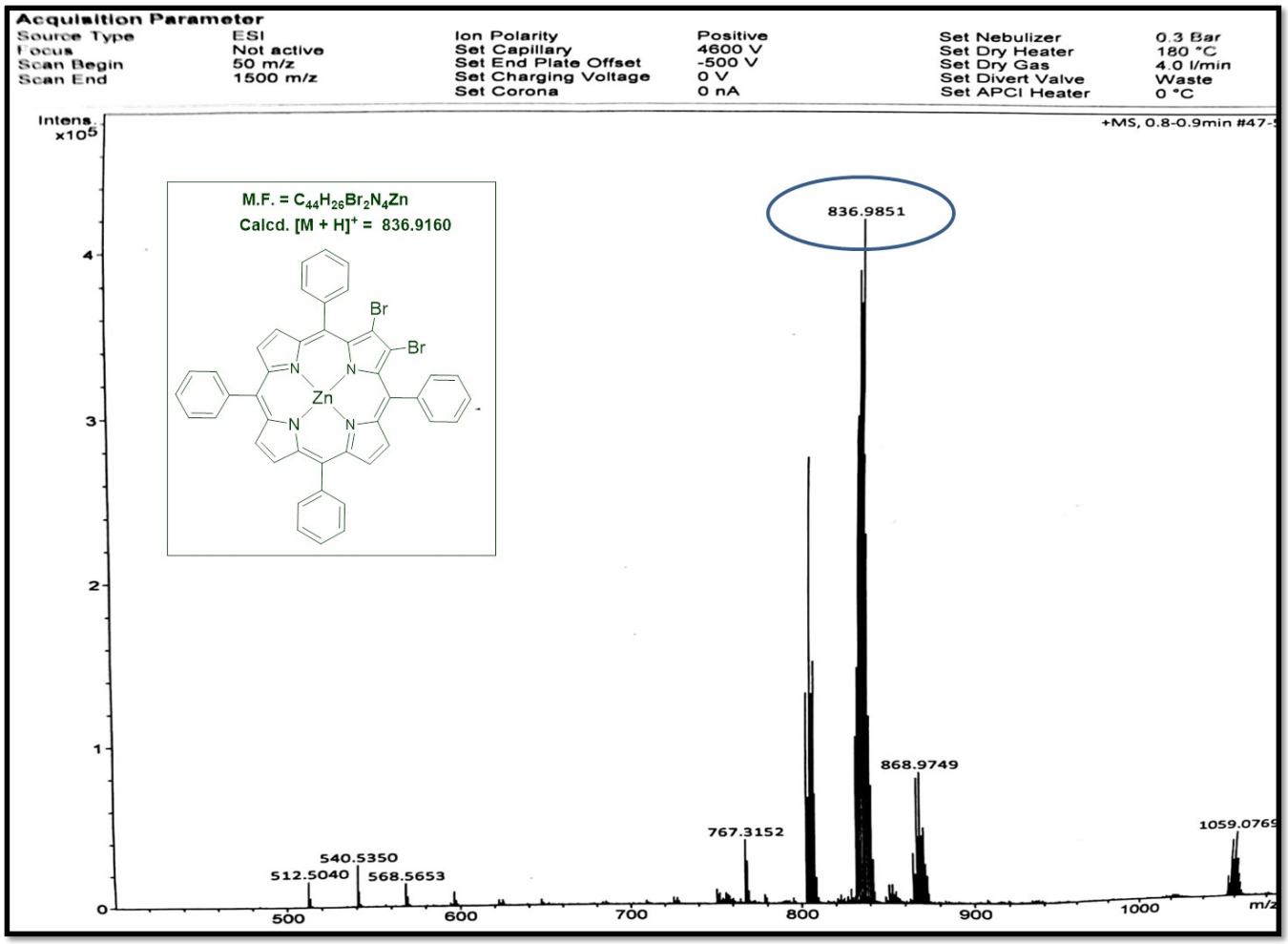

Figure S29. HRMS spectrum of $H_2TPP(CH_3)_2$.

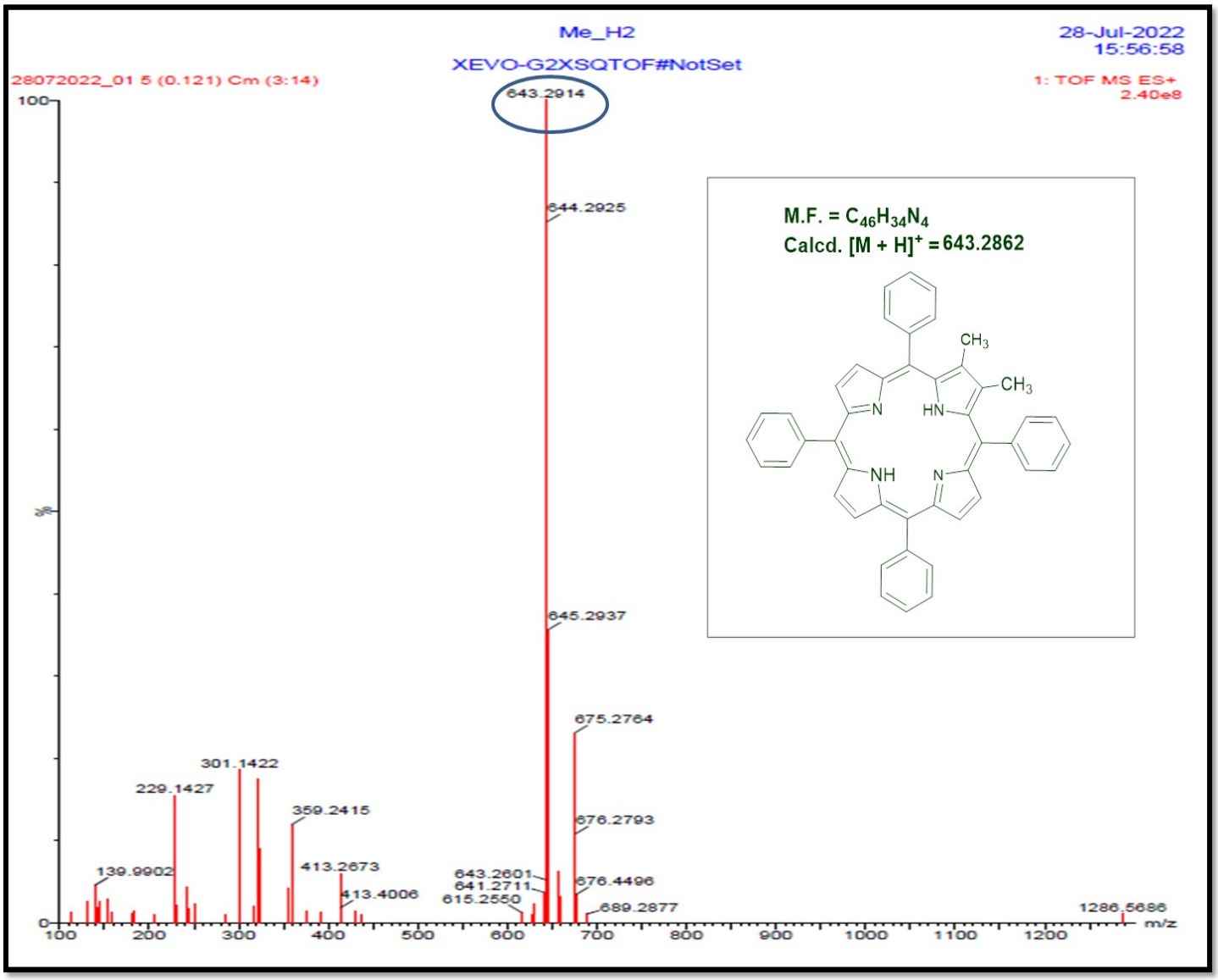

Figure S30. HRMS spectrum of $CoTPP(CH_3)_2$.

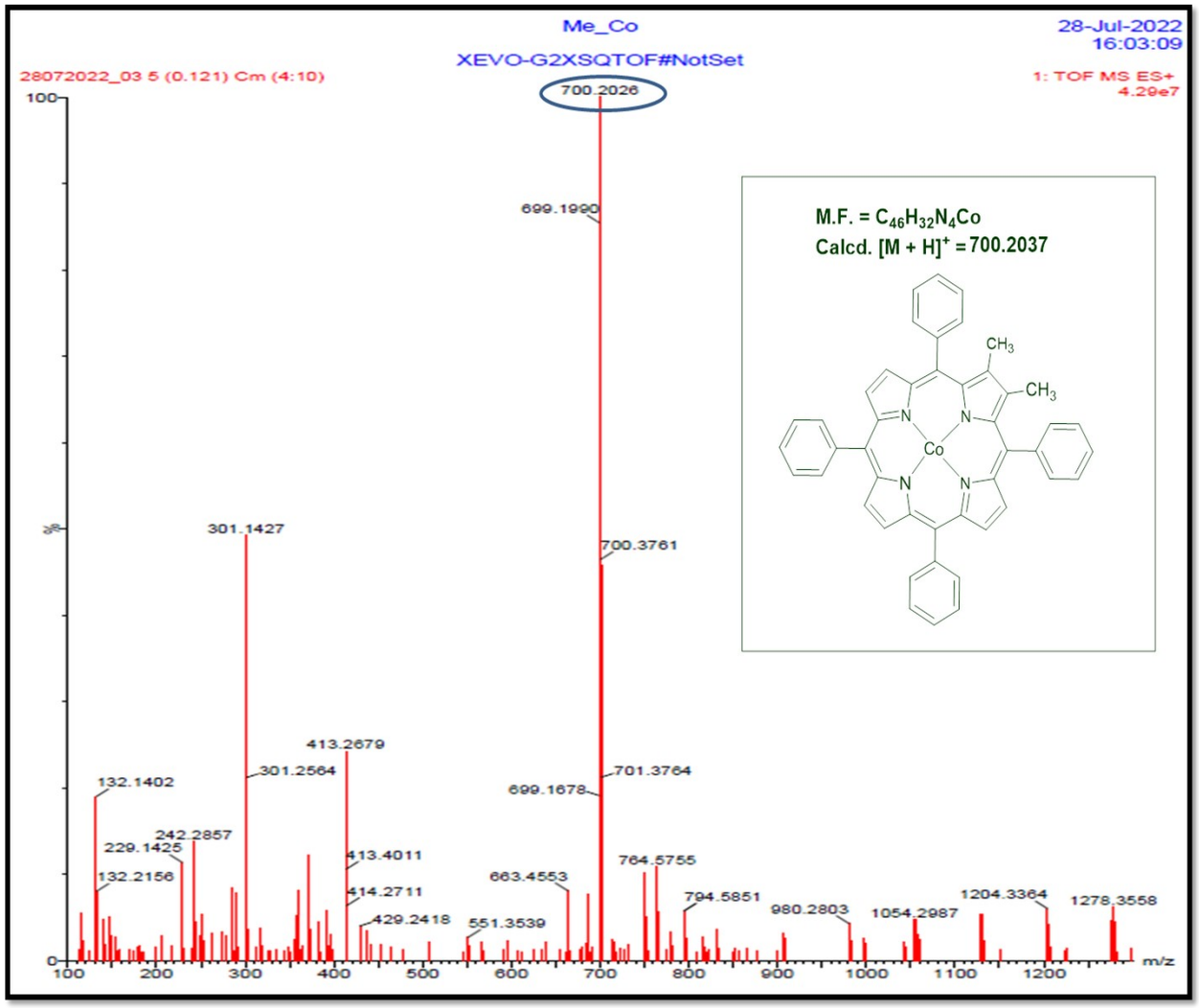

Figure S31. HRMS spectrum of $ZnTPP(CH_3)_2$.

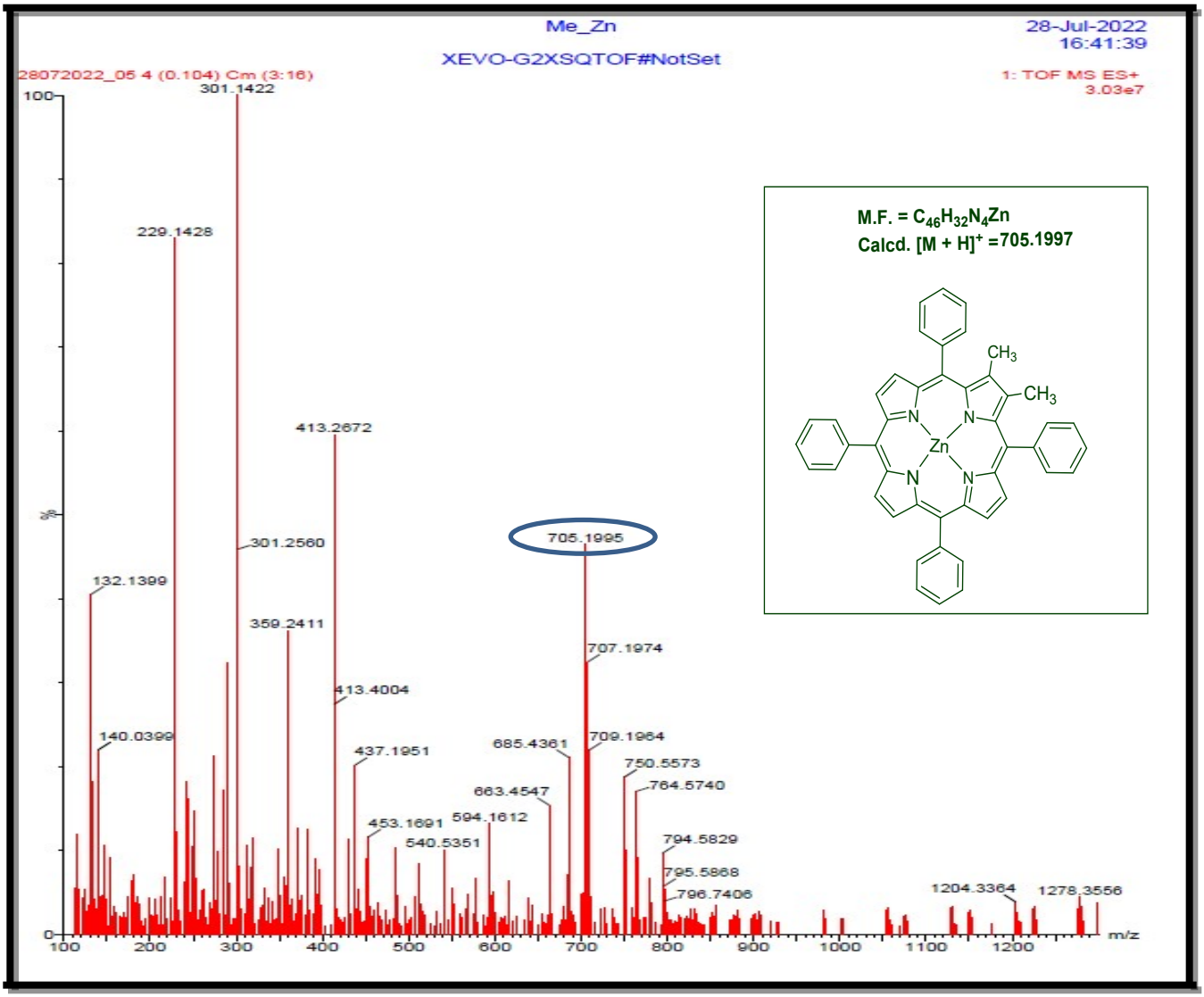

Figure S32. HRMS spectrum of $NiTPP(CH_3)_2$.

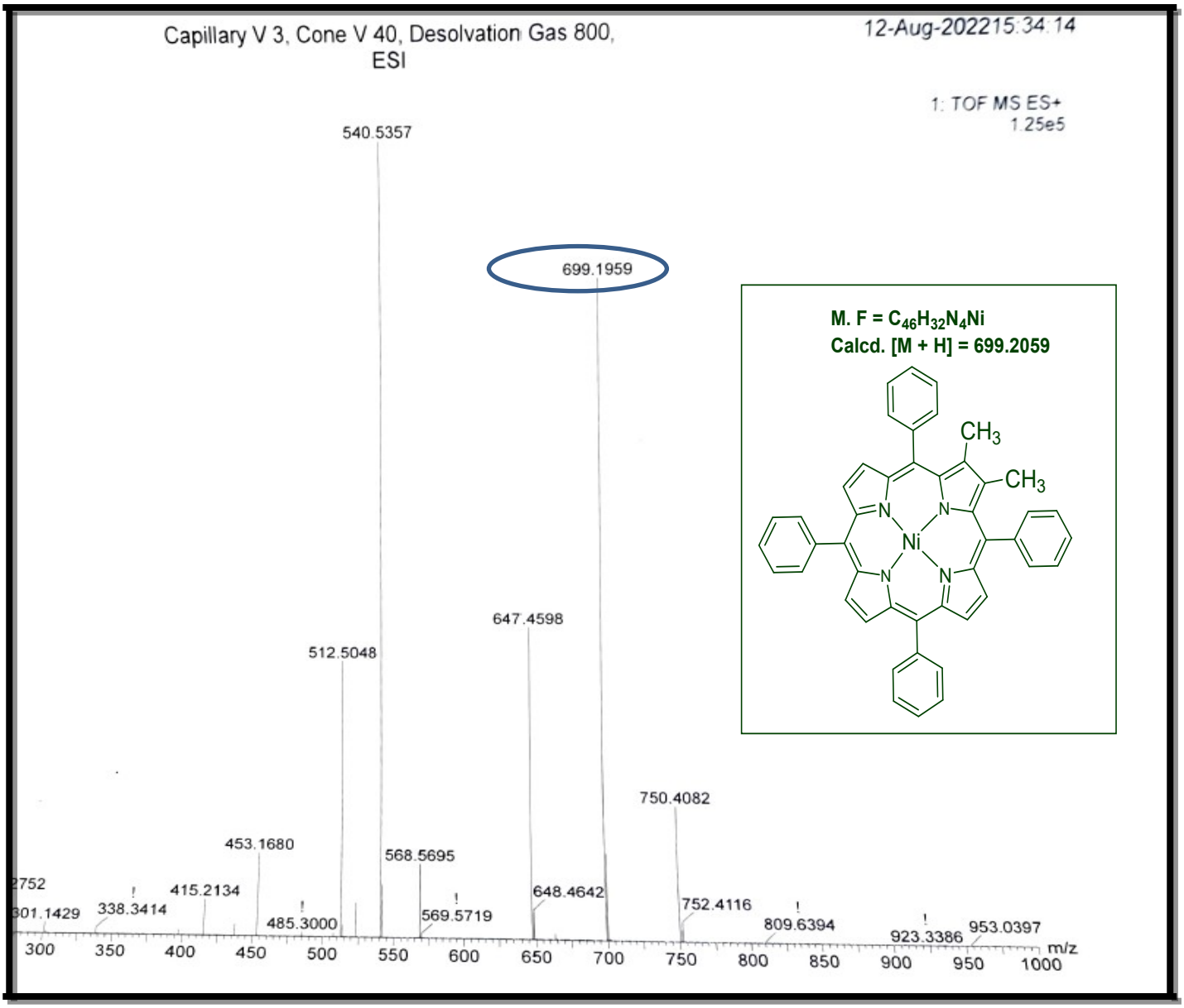

Figure S33. HRMS spectrum of $H_2TPP(PE)_2$.

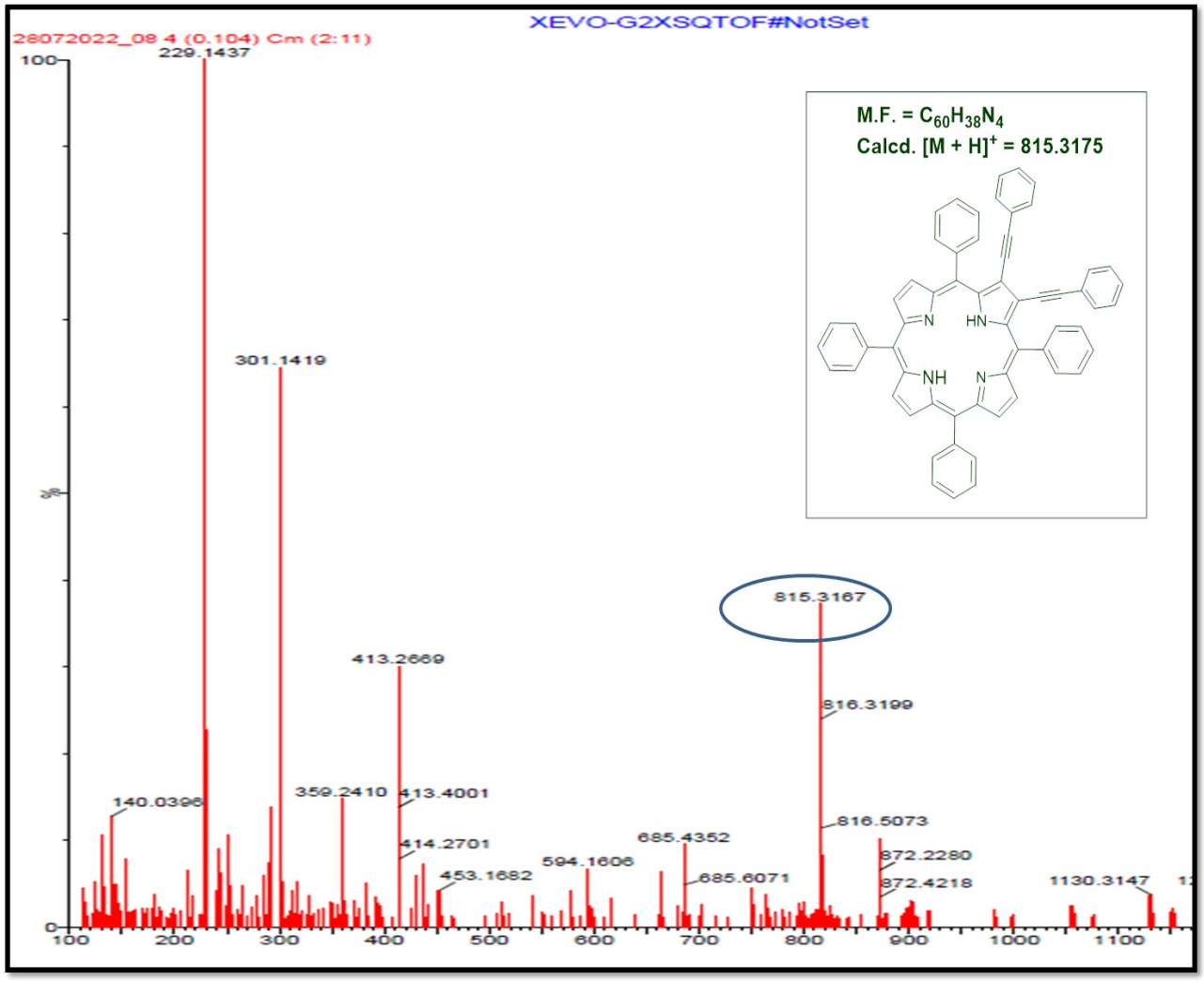

Figure S34. HRMS spectrum of $CoTPP(PE)_2$.

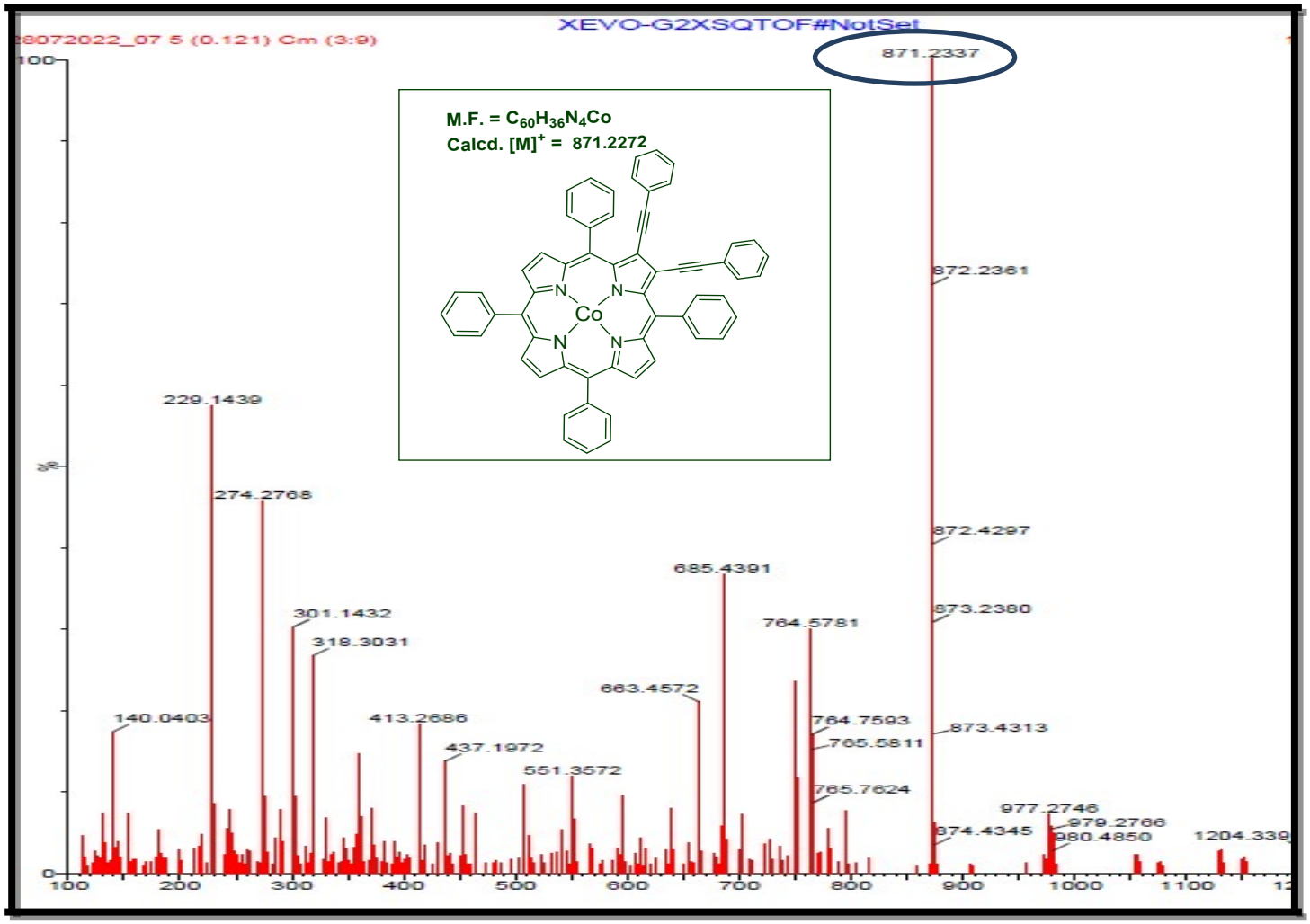

Figure S35. HRMS spectrum of $H_2TPP(Ph)_2$.

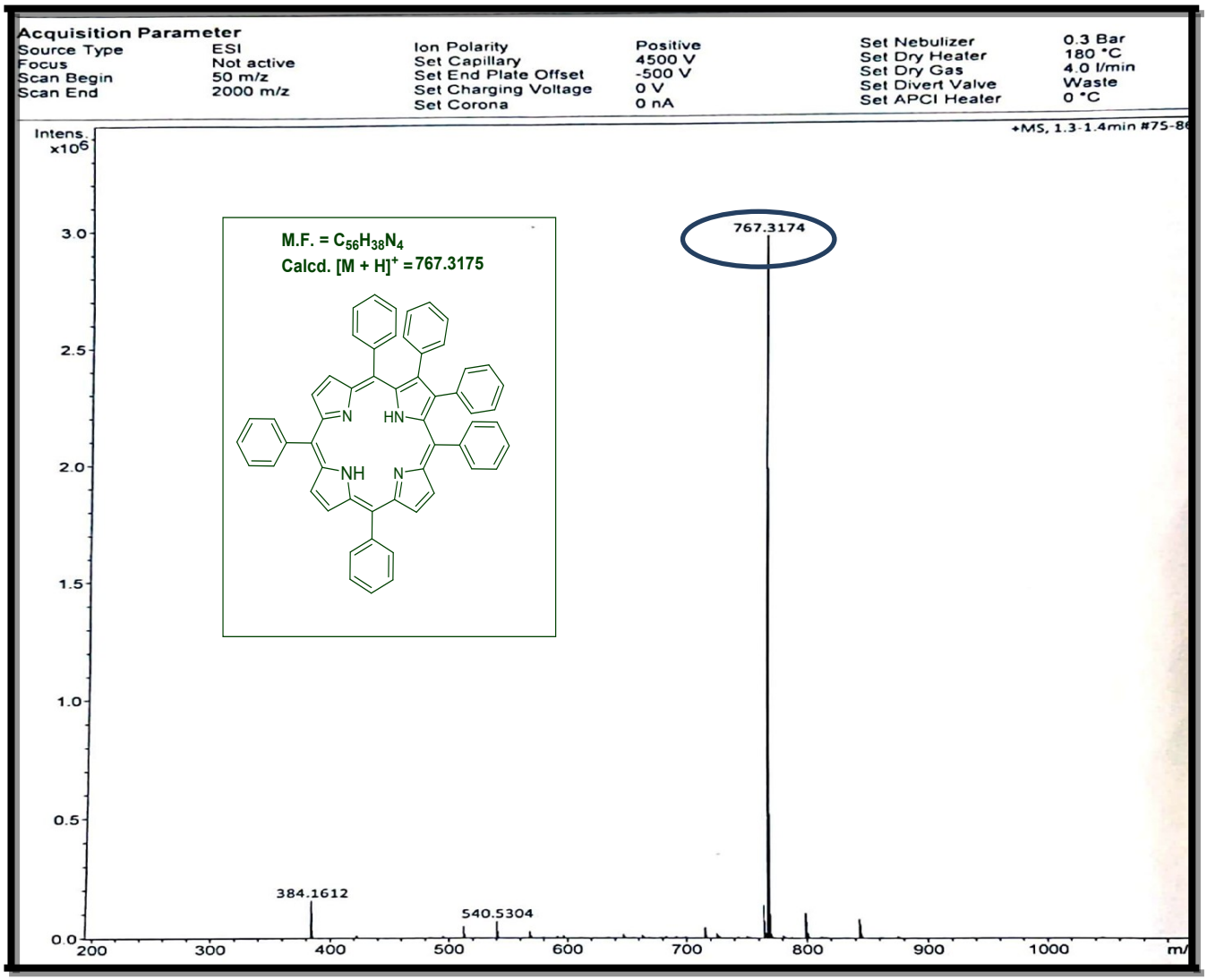

Figure S36. HRMS spectrum of CuTPP(Ph)$_2$.

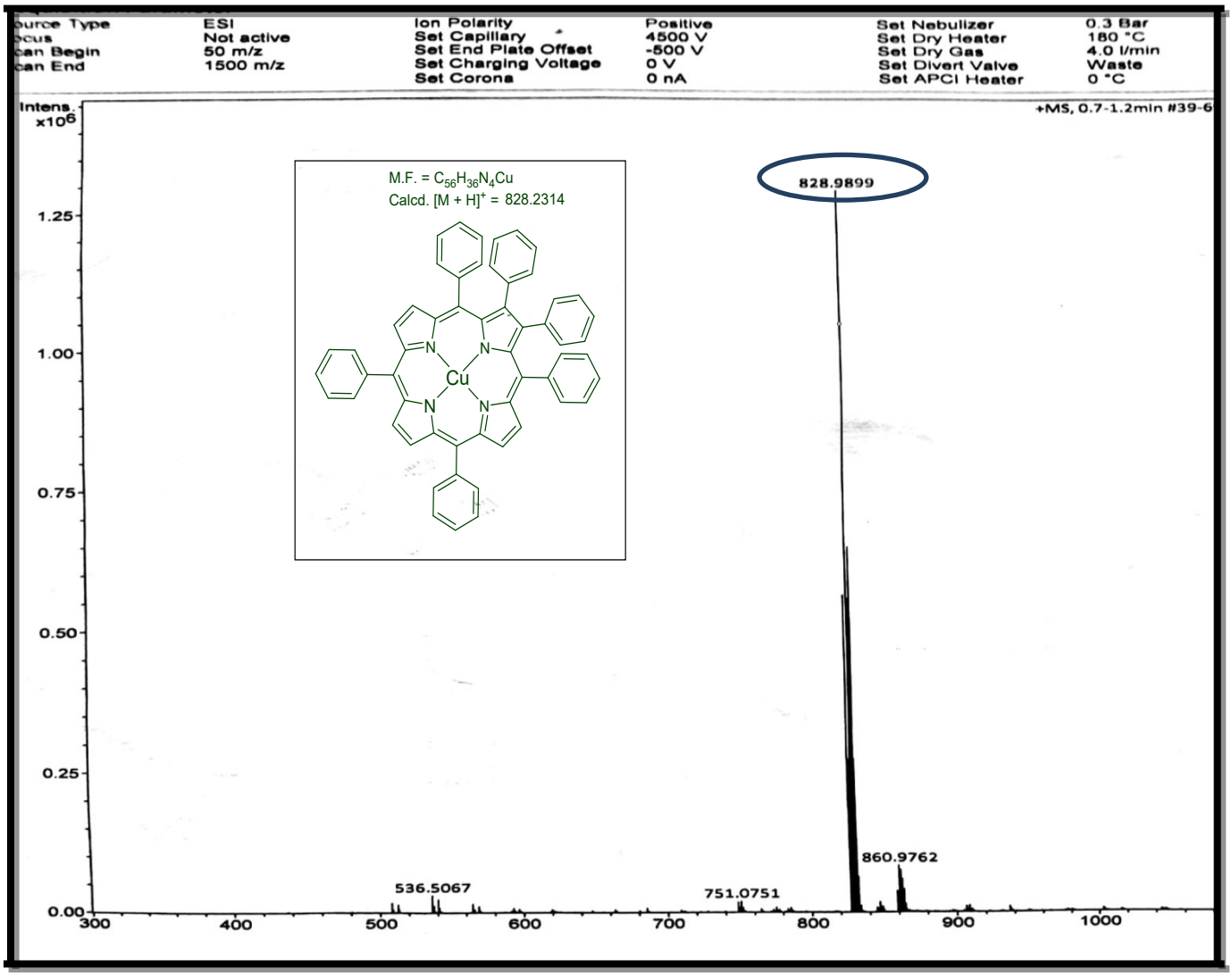

Figure S37. HRMS spectrum of $CoTPP(Ph)_2$.

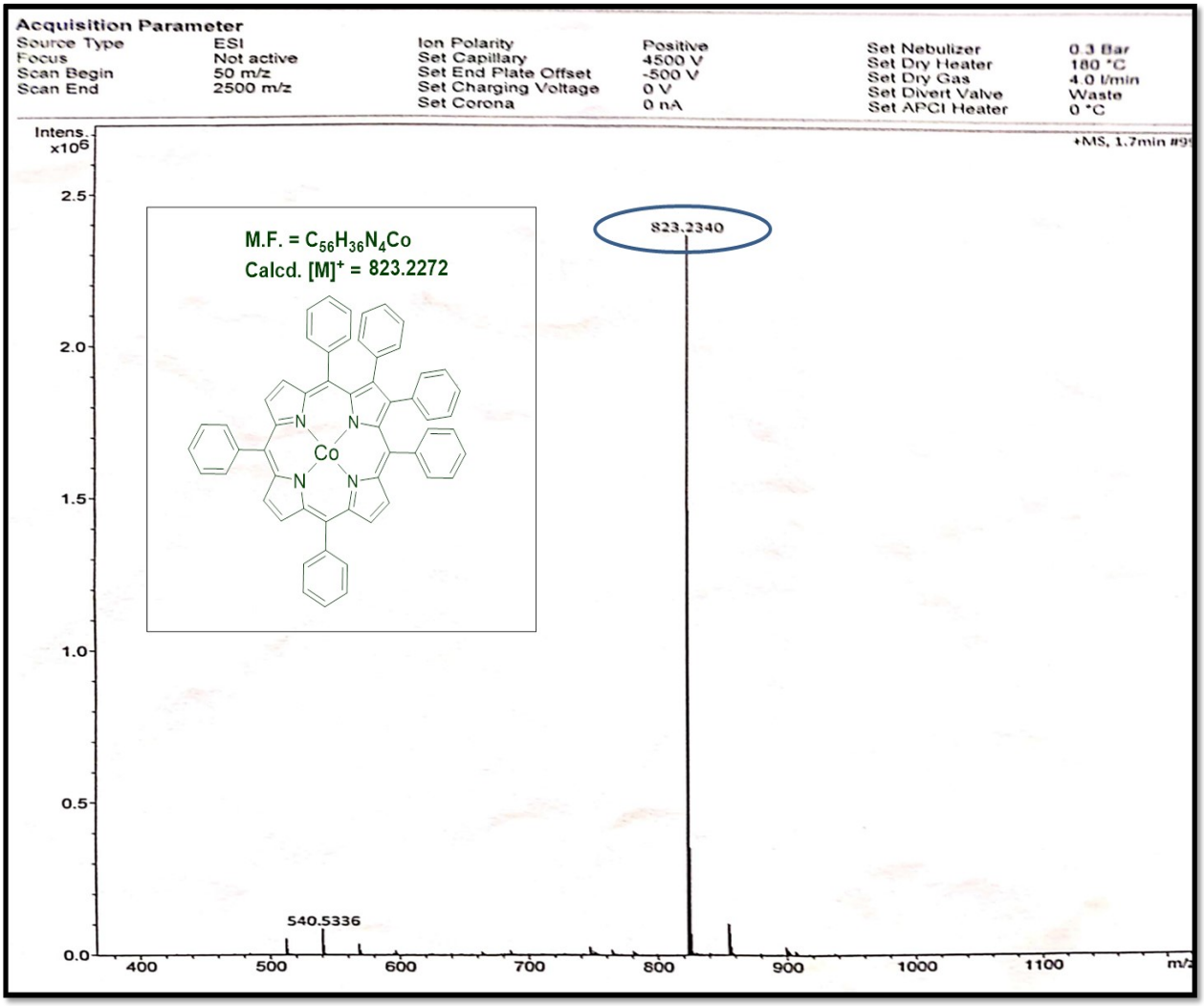
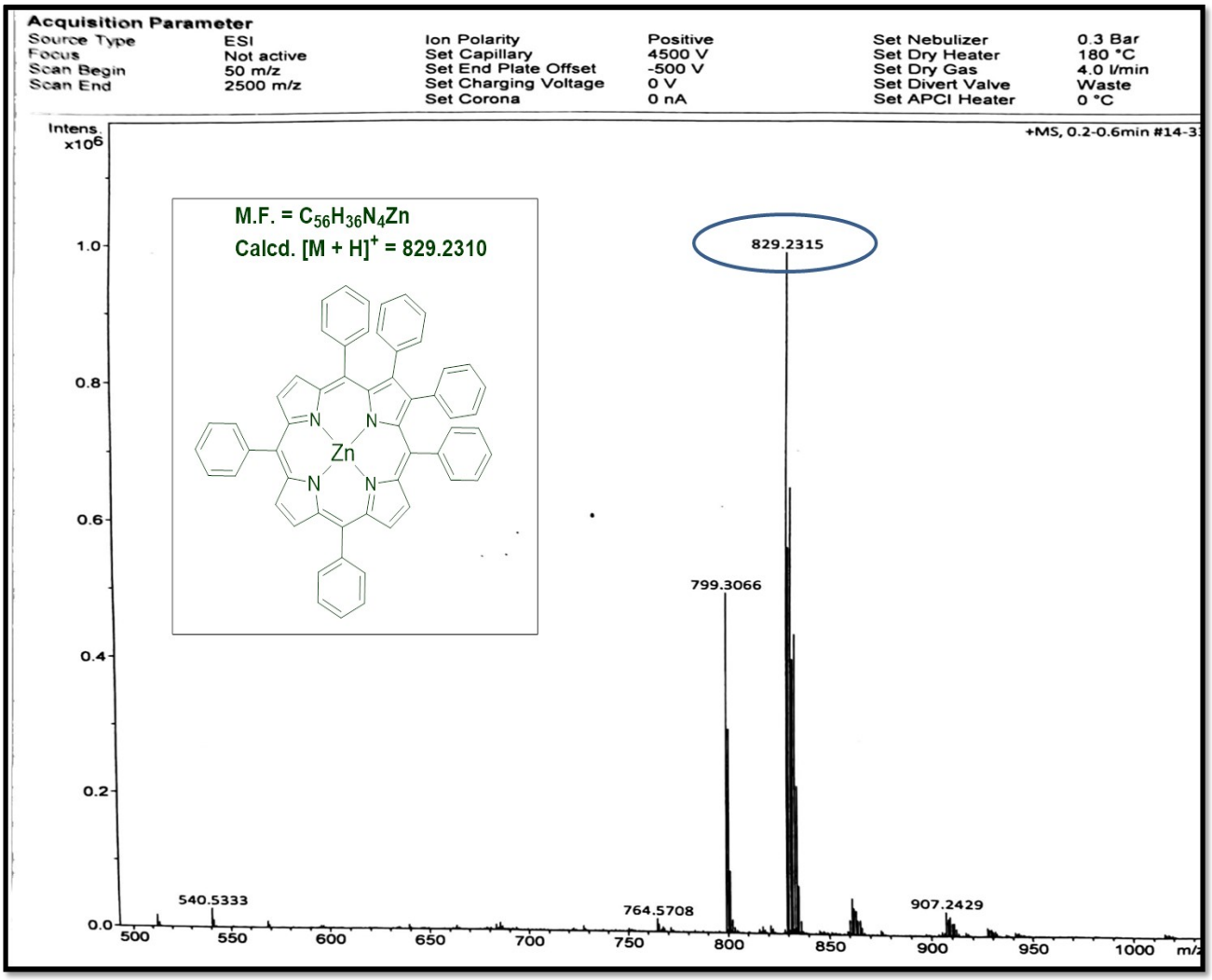
Figure S38. HRMS spectrum of $ZnTPP(Ph)_2$.